Global and Planetary Change 207 (2021) 103648

Contents lists available at ScienceDirect

Global and Planetary Change

journal homepage: www.elsevier.com/locate/gloplacha

Ichnology, sedimentology, and orbital cycles in the hemipelagic Early Jurassic Laurasian Seaway (Pliensbachian, Cardigan Bay Basin, UK)

Grzegorz Pieńkowski [a,*], Alfred Uchman [b], Krzysztof Ninard [b], Stephen P. Hesselbo [c]

[a] Polish Geological Institute–National Research Institute, Rakowiecka 4, PL-00-975 Warszawa, Poland
[b] Jagiellonian University, Faculty of Geography and Geology, Gronostajowa 3a, 30-087 Kraków, Poland
[c] Camborne School of Mines and Environment and Sustainability Institute, University of Exeter, Penryn, Cornwall TR10 9FE, UK

ARTICLE INFO

Keywords:
Hemipelagic contourites
Cardigan Bay Strait circulation
Trace fossils
Orbital forcing
Pliensbachian astrochronology

ABSTRACT

An uncommonly continuous Lower Jurassic (uppermost Sinemurian and Pliensbachian) section (Llanbedr (Mochras Farm) Borehole, Cardigan Bay Basin, UK) comprises hemipelagic calcareous mudstone, wackestone/siltstone and subordinate packstone/sandstone. Some beds show bigradational grading, and their sedimentary structures are typical of contourite drift facies. On the basis of the long-term persistence and stability of the currents that formed these deposits, sedimentation was likely controlled by thermohaline-driven geostrophic contour currents circulating between the Boreal ocean and Peri-Tethys through the narrow and relatively deep Cardigan Bay Basin (Cardigan Bay Strait). Trace fossils are strongly dominated by *Phycosiphon incertum*, which was produced by opportunistic colonizers. *Thalassinoides*, *Schaubcylindrichnus* and *Teichichnus* are common, accompanied by less common *Zoophycos*, *Planolites*, *Palaeophycus*, *Trichichnus* and dwelling structures such as cf. *Polykladichnus*, *Siphonichnus* and *Skolithos*. The ichnofabrics are usually simple, which results from generally high rates of deposition, unstable, water-saturated soft-ground substrate, and the domination of well-adapted *Phycosiphon,* but there are also cyclic appearances of more complex ichnofabrics with dwelling structures, reflecting more stable bottom conditions. A new detailed analysis of the core has allowed cycles to be distinguished based on combination of ichnological and sedimentological features, pointing to distinct cyclicity of oceanographic mechanisms influenced by orbital forcing and driving the inferred fluctuations in benthic life conditions, controlled mainly by variation in contour current intensity and oxygenation of bottom water reflected by trace fossils. The ichnological cycles show four-order hierarchy, which can be attributed to the orbital cycles: precession and obliquity (4th order), short eccentricity (3rd order), and long eccentricity (2nd order). The longest (~ 2.5 Myr) 1st order cyclicity is attributable to the longer "grand orbital cycles" (period related to the Earth–Mars secular resonance), with long-term impacts on palaeoclimatic and oceanic circulation dynamics, and is recorded in large-scale changes in ichnodiversity, correlating with long-term changes of clay minerals and carbonate content. Possibly, there is also ~ 9 Myr cyclicity, expressed in observed modulation of frequency of precession cycles by eccentricity. Harmonic analysis of the cyclicity gives high confidence of orbital signals and allows refined estimation of duration of the Pliensbachian (~8.4 Myr) and the *jamesoni* (~2.8 Myr), *ibex* (~ 2.0 Myr), *davoe*i (~ 0.47 Myr), *margaritatus* (~ 2.33 Myr) and *spinatum* zones (~ 0.8 Myr) with an overall stable sedimentation rate of 4.5–5.1 cm/kyr. Obtained durations show improved fit between 2nd–4th and 1st order cycle and removes the problem of an anomalously long duration and resulting much lower sedimentation rate for the *spinatum* Zone, previously obtained by other methods. A higher diversity of trace fossils is noticed in intervals enriched in smectite; most likely, this clay mineral occluded pore spaces and limited the competition from the opportunist *Phycosiphon* makers, allowing development of other, more specialized forms. The continuous, expanded ichnological record of deep-water hemipelagic/contour drift sediments is sensitive to climatic and oceanographic changes controlled by orbital cycles. The Cardigan Bay Strait played an important role in the Early Jurassic (at least Pliensbachian) oceanic circulation, providing a major link between the northern and southern part of the Laurasian Seaway (and in general between the Boreal and Peri-Tethys domains), funneling currents flowing from the north to the south.

* Corresponding author.
E-mail addresses: grzegorz.pienkowski@pgi.gov.pl (G. Pieńkowski), alfred.uchman@uj.edu.pl (A. Uchman), k.ninard@doctoral.uj.edu.pl (K. Ninard), S.P.Hesselbo@exeter.ac.uk (S.P. Hesselbo).

https://doi.org/10.1016/j.gloplacha.2021.103648
Received 15 June 2021; Received in revised form 27 August 2021; Accepted 16 September 2021
Available online 22 September 2021

1. Introduction

The Llanbedr (Mochras Farm) borehole (hereafter referred to as Mochras) cored the Lower Jurassic of the Cardigan Bay Basin (Wales, UK), an extensional structure related to the break-up of Pangaea. During the Early Jurassic, the basin was located at a mid-palaeolatitude, on the NW fringe of the European shelf, in the Laurasian Seaway (Figs. 1, 2). The core has been studied in many respects, including biostratigraphy (the core was calibrated to a zonal or even subzonal level using ammonites), lithology (Woodland, 1971; Dobson and Whittington, 1987; Hesselbo et al., 2013; Copestake and Johnson, 2014), marine plankton (Van de Schootbrugge et al., 2005), clay minerals (Deconinck et al., 2019; Munier et al., 2021), and astrochronology (Ruhl et al., 2016; Storm et al., 2020).

The uppermost Sinemurian-Pliensbachian (Lower Jurassic) section of the Mochras core represents the most expanded and highest resolution cyclostratigraphic dataset for the Pliensbachian to date, and provides the most reliable basis for an astrochronological time scale, reflecting Milankovitch forcing, predominantly at precession/obliquity and the short- and long-eccentricity periodicities (Figs. 3, 4). The dominant expression of the medium-amplitude Carbon Isotope Excursions (CIEs) in Mochras testifies to the expanded stratigraphic resolution and relative completeness of sedimentary record therein, allowing distinction between intrinsic Earth processes and extrinsic solar system dynamics such as the driving mechanism for the Early Jurassic $\delta^{13}C$ fluctuations (Storm et al., 2020).

Astronomical duration of the Pliensbachian, based both on dominant spectral peaks in elemental Ca and Ti in lithology and geochemical palaeoenvironmental proxies (Ruhl et al., 2016) or carbon isotope fluctuations (Storm et al., 2020), was estimated at about 8.7–8.8 Myr, although durations of successive ammonite zones were slightly different in the two studies. Generally, fossils and lithology point to a consistently fully marine hemipelagic setting (Ruhl et al., 2016). In addition, climate changes have been interpreted on the basis of clay minerals (Deconinck et al., 2019) and organic geochemistry (Storm et al., 2020). However, a more focussed characterization of sedimentary environment, ichnology and benthic life conditions has not yet been carried out.

Herein, we present detailed sedimentological and ichnological analyses, which allow recognition of ecological parameters on the basis that trace fossils are sensitive in situ indicators of even very subtle environmental changes such as current strengths, oxygen content, food supply, and stability of the environment (Savrda, 1995; Savrda and Bottjer, 1994). Benthic invertebrates respond to various environmental changes driven by orbital forcing (e.g. Wetzel, 1991; Erba and Premoli Silva, 1994; Hüneke and Stow, 2008; Pervesler et al., 2008; Rodríguez-Tovar et al., 2011; Rebesco et al., 2014; Rodríguez-Tovar, 2014; de Castro et al., 2020b), but the mechanisms of control (Valdes and Glover, 1999; Paillard, 2010) are still poorly understood. In this paper, we present an analysis of lithological and ichnological cycles related to the orbital cycles and a refined estimation of the astronomical duration of the Pliensbachian and the ammonite zones within this stage.

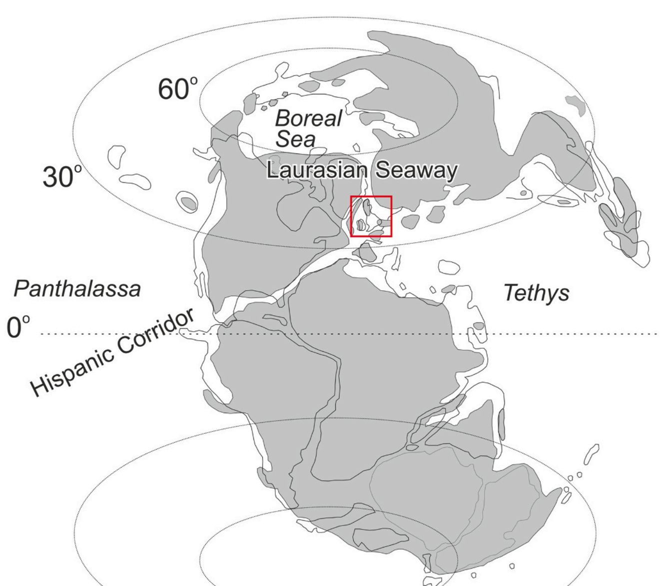

Fig. 1. Pliensbachian palaeogeography with locality of the Laurasian Seaway and Mochras borehole (modified from Dera et al., 2011 and Korte et al., 2015).

2. Material and methods

A nearly continuous 420 m-thick section of core (< 4 m missing), was investigated using standard sedimentological logging at a centimetre-scale accuracy (Figs. 3–10) with special attention paid to the integration of sedimentological and ichnological observations. Dunham's (1962) classification of carbonate rock lithotypes was adopted as it centres on depositional texture and is well suited for macroscopic observations (employing a hand lens or binocular microscope). Additionally, 93 thin sections (approximately one thin section for every 4–5 m of core) were examined for recognition of microfacies and lithology.

For the needs of the numerical cyclicity analysis, occurrences of trace fossils *Phycosiphon*, *Thalassinoides* and *Schaubcylindrichnus* (Figs. 5, 6, 8–10), as well as intervals with preserved lamination within the sedimentary log were treated as discrete binary time series. Ranges of trace fossils and lamination were manually digitized with an even step of 10 cm, resulting in the time series consisting of approximately 4200 binary digits each (Supplementary 1).

To statistically verify whether particular trace fossils and lamination occur non-randomly, the runs test has been applied (Supplementary 2). The non-parametric runs test evaluates the null hypothesis that two states are distributed randomly in a binary time series (Hammer and Harper, 2006). For the needs of this study, the hypotheses adopted are:

H_0: distribution of occurrences is random;

H_1: distribution of occurrences is non-random.

Runs are defined as uninterrupted sequences of either occurrence (N_1) or non-occurrence (N_2) of particular trace fossil or lamination. Statistically significant discrepancy between the observed number of runs (R) and the number of runs expected in case the time series were random ($\bar{R}$) allows rejection of the null hypothesis. The test statistic Z has been computed using the runs test module of PAST 3.2 software (Hammer et al., 2001) separately for each studied ichnotaxa and lamination. Absolute values of resultant *Z*-scores have been compared to the critical value of 1.96 corresponding to 5% significance level in a standard normal table.

Binary time series can be considered to represent a sum of component constant-frequency waves. The transform operation can be applied to extract the frequency spectrum of the component waves. Various numerical methods derivative of the Fourier transform, while commonly applied in the analysis of continuous time series, are inappropriate to analyze binary time series (Weedon, 2003). Power-spectral analysis based on the Walsh transform is considered to be the most correct method of finding periodicities within such time series. The Walsh transform outputs the spectral data as a function of sequency, defined as half of the average number of zero transitions per unit of time or space. In terms of the interpretation of results, the sequency of the Walsh domain coincides with the commonly recognized concept of frequency. Theoretical background behind the Walsh technique and its applicability in time series analysis have been provided by Negi and Tiwari (1984), Weedon (1989), Weedon and Read (1995), van Echelpoel (1994) and Maiti and Tiwari (2012). The studies of Tiwari (1987) and Negi et al. (1993) demonstrate that besides the main orbital cycles, the Walsh power-spectrum displays component periodicities, beat periodicities, and combined effects of other periodicities, theoretically predicted by Berger (1977).

Occurrences of selected trace fossils and intervals with preserved lamination have been subjected to spectral analysis using the Walsh transform module of PAST 3.2 software (Hammer et al., 2001) (Tables 1, 2; Figs. 11, 12). The terminations of the time series were experimentally adjusted to obtain the optimal balance between the signal-to-noise ratio and spectral resolution. The spectral analysis outputs the power-spectra as a function of stratigraphic thickness – i.e. number of cycles per one metre (Fig. 11). The obtained spectrograms were converted from the thickness domain into the time values based on the average sedimentation rate adopted as 4.7 cm per 1000 years. This sedimentation rate was tuned for *jamesoni* Zone to the 405 kyr cycles (Ruhl et al., 2016). Independently, similar long-term sedimentation rate estimates (4.9 cm/kyr) can be obtained by dividing the combined thickness of *margaritatus* and *spinatum* zones in Mochras (147 m) by approximate duration of these zones (~ 3 Myr), based on radiometric dates from Oregon, USA (De Lena et al., 2019). Thereby, the deposition of one-metre-thick sediment interval took 20,770 years on average. The time values corresponding to individual peak sequency values were calculated as a proportion of 20,770 years. For a comparison, the conversion was also tested with 4.4 and 4.5 cm/kyr sedimentation rates (obtained herein for *jamesoni* and *ibex* zones), which resulted in very similar values and did not influence the interpretation of the cycle duration.

3. Results

3.1. Lithology and sedimentary structures

The succession primarily comprises calcareous mudstone/micrite, wackestone and grainstone with varying calcareous grains of silt to fine-sand size. Siliciclastic contribution in coarser silty-sandy lithofacies is weaker, usually between 10 and 30%, while the mudstone contains a greater siliciclastic component and locally (1232 m, 988 m and 865 m) is carbonate-free (Figs. 3, 4; Ruhl et al., 2016). Macrofossils are represented mainly by pelagic cephalopods. Widespread crinoid ossicles are most likely redeposited from shallower settings due to their buoyancy (Savarese et al., 1997). Benthic shelly organisms are rare on the slabbed core surfaces, and are represented by in situ burrowing bivalves found in a few horizons (Fig. 10E). Fossil collections made from the "working half" broadly confirm this distribution (Woodland, 1971; Ullmann et al., 2021). Benthic foraminifers are present as well (Copestake and Johnson, 2014). Drifted flora occurs locally, mostly in the *ibex* and *davoei* zones. Lamination and low-angle cross lamination are common, particularly upwards from the *ibex* Zone. Carbonate-rich parts (uppermost *jamesoni* Zone, and in particular the upper *margaritatus* and the lowermost part of *spinatum* zones) suggest early diagenetic processes, such as calcite cementation and formation of calcite nodules (Figs. 5D, 6A), which may result from the degradation of organic matter and the associated reduction of sulphates (Ruhl et al., 2016). Nodules are surrounded by

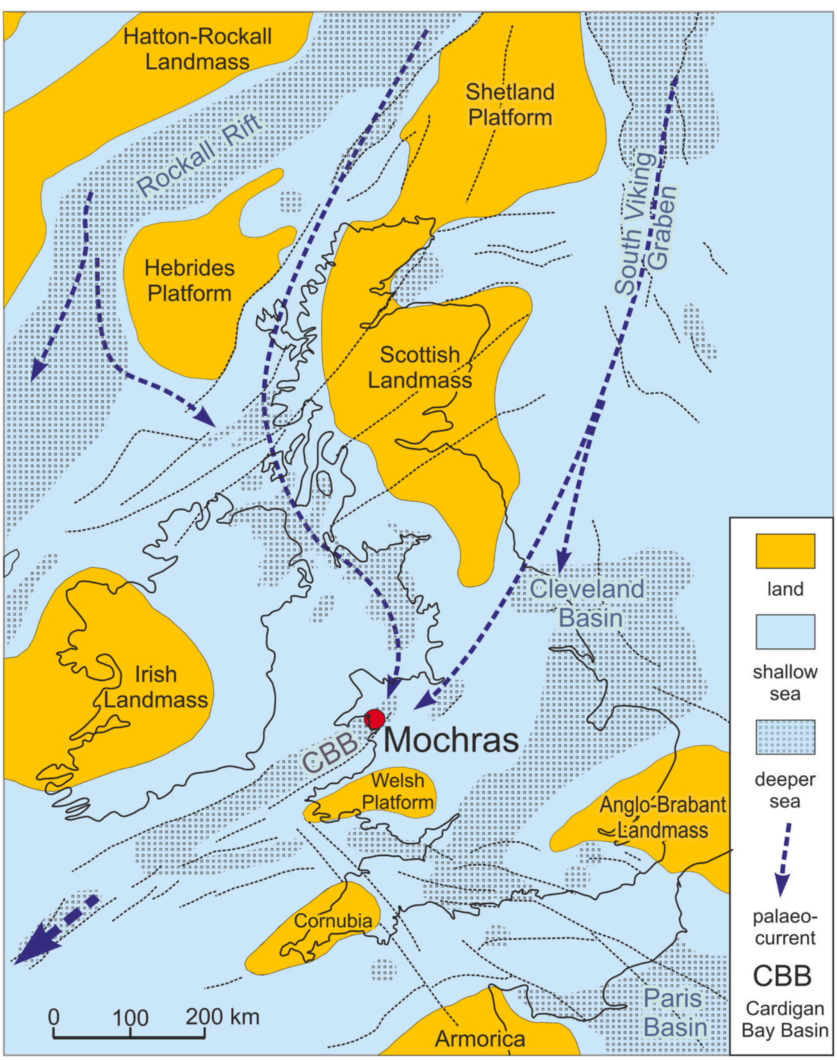

Fig. 2. Enlargement of the area in the frame (Fig. 1) showing major basins and elevated areas in the Pliensbachian times (after Cope et al., 1992 and Raine et al., 2020, amended). Note the inferred current flow paths with several alternatives – while all of them seemed to be possible for the early Pliensbachian, for the late Pliensbachian that flow must have been predominantly through more westerly seaways, likely Faeroe – Rockall Rift, because in the late Pliensbachian sands are shed off a central North Sea uplift into the Cleveland Basin and other circum North Sea basins and in the Hebrides (W Scotland). Note the pivotal position of the Cardigan Bay Strait (now Cardigan Bay Basin – CBB) in the Laurasian Seaway between Boreal Sea and Peri-Tethys domain, funneling water flows from the north.

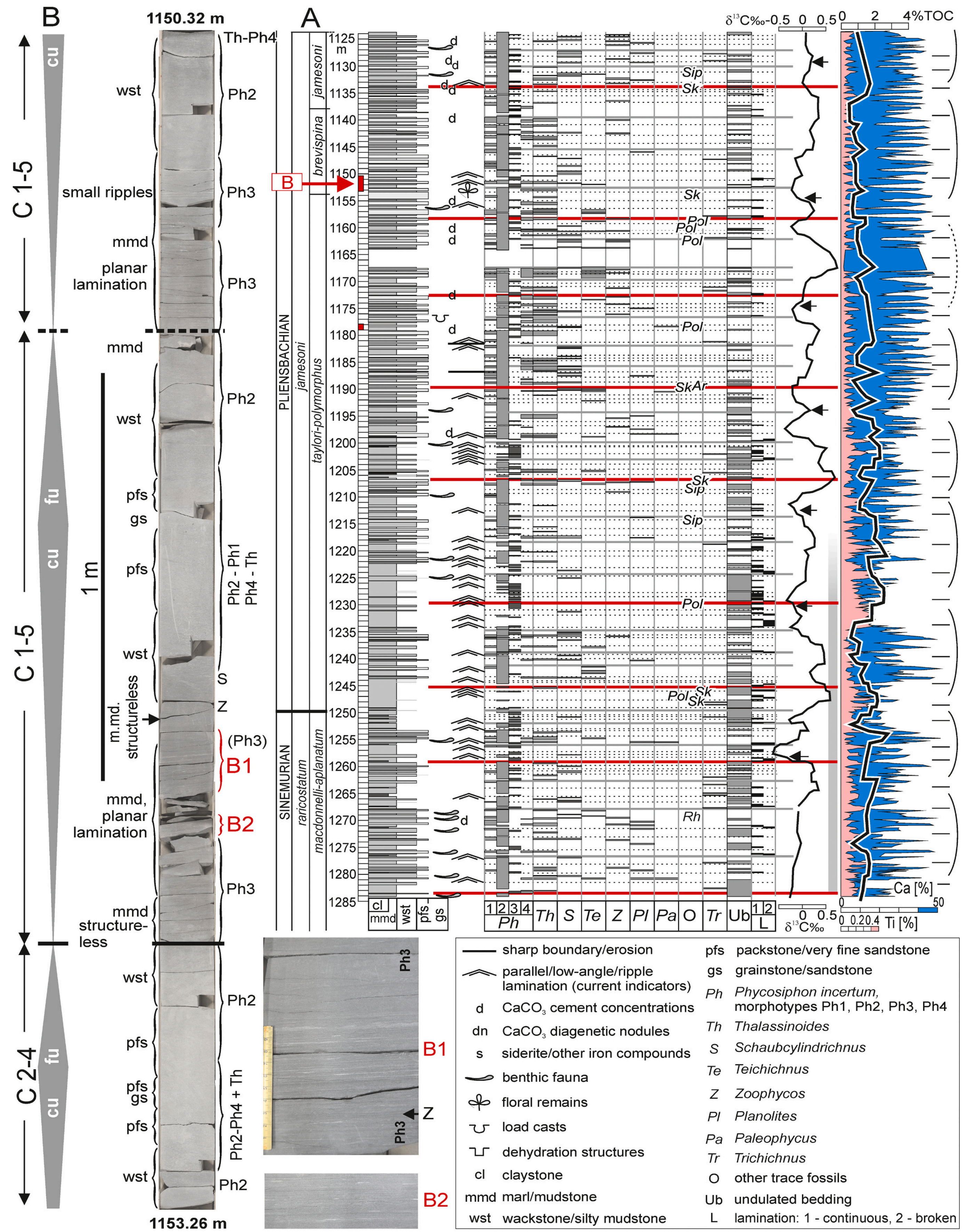

(caption on next page)

Fig. 3. Investigated part of the Mochras Borehole. A – Panel showing stratigraphy (stages, ammonite zones and subzones), lithology, ichnology and geochemistry of the uppermost Sinemurian and lower part of the Pliensbachian section of the Mochras borehole (1123.8–1284.5 m). O. – other, rarely occurring trace fossils: *Ar* – *Arenicolites*; *Ast* – *Asterosoma*; *Mon* – *Monocraterion*; *Phy* –?*Phymatoderma*; *Pol* – cf. *Polykladichnus*; *Rh* – *Rhizocorallium*; *Sip* – *Siphonites*; *Sk* – *Skolithos*. *Trichichnus* (filamentous mat-forming, sulfide-oxidizing bacteria and "pyritized tubes") represent traces of unidentified life activity/disputable origin. Ub – micrite/mudstone of 'massive' appearance, with undulated or cuboid parting. Geochemistry: $\delta^{13}C_{TOC}$ – carbon isotope curve, scale −0.5–0.5‰; TOC, scale 0–4% (after Storm et al., 2020); XRF-derived calcium and titanium record (after Ruhl et al., 2016). Cyclicity: thin dashed lines – 4th order (c. 20 kyr) cycles; solid grey lines – 3rd order (c. 100 kyr) cycles; red lines – 2nd order (c. 405 kyr) cycles; grey bar on the right – 1st order (c. 2.5 Myr) cycles, approximately corresponding also to Ca/Ti trends (Ruhl et al., 2016) and clay mineral changes (Deconinck et al., 2019). Arrowed – $\delta^{13}C_{TOC}$ 405 kyr cycles after Storm et al. (2020); Ca – Ti 100 kyr cycles (short lines) and 405 kyr cycles (arches) interpreted by Ruhl et al. (2016). Red bars in the metric depth column – position of the section presented to the left in Panel B and section 1177.98–1178.97 m presented in Fig. 5. B – typical sedimentary cycles occurring in the Pliensbachian stage of Mochras (section 1150.32–1153.26 m, arrowed as "B" section in the panel "A"), showing bigradational (symmetrical) cycles, with gradually coarsening upward (cu) and gradually fining-upward (fu) phases. Note the pinstripe, calcareous mudstones (B1 detail photograph), interlaminated with calcareous/silty lamina and incipient, small ripples – the latter are interpreted to be deposited by weak currents, under more oxygenated conditions than massive structureless and laminated or "massive" mudstones. Micrite-mudstone (m.md.) facies contain only sparse *Phycosiphon incertum* type 3 or indistinguishable minute bioturbation structures produced by meiofauna in structureless, "massive" calcareous mudstones (see Fig. 6.5). In a thin, laminated mudstone section (B2 detail photograph) meiofaunal bioturbation structures are missing, which points to intermittent oxygen deficiency. *Zoophycos* (*Z*) occur at the facies boundary between mudstone and wackestone and *Schaubcylindrichnus* (*S*) slightly above. The coarser and more carbonate-rich facies comprising packstone-very fine sandstone (pfs) and grainstone-sandstone (gs) is thoroughly bioturbated with *Phycosiphon incertum* and subordinately *Thalassinoides*. Cycle boundaries are determined based on ichnofabric and lithology – heavy line – 3rd order cycle boundary, dashed line – 4th order cycle boundary. Current-generated structures (such as pinstripe lamination and small current ripples) and characteristic bigradational ("symmetrical") cycles with bioturbated coarser parts result from variations in current velocity. C1–C5 cycles represent "full" contourite cycles, and the incomplete C2–C4 cycle, with its lowermost and uppermost parts missing are referred to as contourite cycles (Stow et al., 2002; Stow and Faugères, 2008 – see also Figs. 5–7). (For interpretation of the references to colour in this figure legend, the reader is referred to the web version of this article.)

more ductile, uncemented mudstone, which is deformed around them. However, conspicuous condensation/cementation levels with a hard crust are absent. Dewatering/compactional cracks are observed only in a few horizons (Fig. 10M).

Six main lithofacies types (Fig. 7) are identified in the Mochras section: (1) Dark grey, planar-laminated siliceous-calcareous micritic mudstone and siliceous claystone; bioturbation structures are typically not observed, but in silty parts small horizontal burrows are present; therefore, two sub-lithofacies were distinguished: with continuous (Figs. 3B2, 9A) and broken lamination (Fig. 9B); (2) "massive", poorly bedded mudstone/carbonaceous micritic mudstone, in some cases showing centimetre- to decimetre-scale banding with faint, slightly undulated or cuboid parting, which is connected to homogenization by meiofaunal bioturbation of sub-millimetre size; in places, peloidal structure occurs; discrete trace fossils are relatively rare (Fig. 9E); (3) "pinstripe" carbonaceous mudstone that is laminated with wackestone-siltstone, in which planar laminae are often discontinuous and lenticular to wavy, planar parallel, or low angle cross-lamination, starved ripples are present, and bioturbation structures can obliterate these in mottled mudstone-wackestone (Figs. 3B1, 9C, D); (4) interlaminated, heterolithic siltstone or wackestone with mudstone, usually bioturbated, with only local sedimentary structures; this lithofacies shows irregular arrangement of mudstone, wackestone-siltstone or grainstone-sandy siltstone in pockets, lenses and streaks, and less commonly, a rapid alternation of thin irregular layers of these three lithologies (Figs. 5A, B; 6A); (5) packstone/siltstone to very fine sandstone, with primary sedimentary structures - usually obliterated by bioturbation - including parallel bedding and small-scale cross-bedding (Fig. 9H); (6) sandstone-grainstone, usually bioturbated, with primary structures (parallel bedding and small-scale, low-angle cross-bedding) observed in some horizons (Figs. 4C, 9D).

Contacts between these different lithofacies may be either gradational, yielding indistinct bedding (Figs. 3B, 5B, 6B, 9H), or sharper due to the erosive action of relatively stronger bottom currents (Gross and Williams, 1991), thereby yielding more distinct bedding (Figs. 5C, 6A, 10N). However, sharp bed boundaries in the Mochras Pliensbachian section are rare and evidently not associated with significant hiatuses or erosion, which might be expected to be marked by induration of the sediment surface, or occur as semi-consolidated/firm muddy substrates with sharp-walled, unlined, uncompacted passively filled burrows exhibiting scratch traces along the walls underneath these boundaries.

Lithofacies types 1–6 (Fig. 7) and related ichnofabric in Mochras are not arranged randomly, but appear in a cyclical order (Figs. 3-7). Fully developed, usually 0.5–3 m thick bigradational grading sequences (referred to as "couplets" by previous authors) commonly begin from mudstone lithofacies type 2 (representing mixed layer, mottled by burrowing activity of meiofauna, or mudstone lithofacies type 1 (laminated), passing gradually into lithofacies type 3 – pinstripe mudstone with ripple-drift cross laminated siltstone, or lithofacies 4 – bioturbated mudstone-wackestone, followed by usually bioturbated wackestone-siltstone and packstone-grainstone with traces of stronger currents (Fig. 9D, H). Above this coarsening-upward part is a fining-upward suite, developed in reversed order, although less complete; usually only lithofacies types 6–5–4 are present. This fining-upward phase of the sequence is usually thinner compared to the coarsening-upward phase (Figs. 3B, 7). In many cases the whole sequence is incomplete; either top or bottom parts can be missing (bottom cut-out cycles or top cut-out cycles – Figs. 7, 5C, D, 6A). Additionally, internal erosion surfaces in some of the coarser parts occur (Figs. 5C, 10N), although they are generally rare in the Pliensbachian profile, with relatively more frequent occurrences only in few intervals – in the mid-*ibex*, upper part of *margaritatus* and the lowermost part of *spinatum* zones (Figs. 3, 4). Of note is the ~5 m-thick interval in the uppermost *spinatum* Zone with homogenous carbonate-free mudstone, traces of iron compounds (Figs. 4, 6B), and distinct clay mineral assemblage of mixed-layer clay minerals with berthierine and detrital kaolinite (Deconinck et al., 2019).

3.2. Trace fossils, ichnofabrics

Trace fossils exhibit sharp outlines and possess a characteristic recurrent geometry that allows their classification in terms of ichnotaxonomy, while bioturbation structures have less distinct outlines and do not display a recurrent geometry (Wetzel and Uchman, 2012). Below, they are briefly described in the alphabetic order.

Arenicolites (Fig. 10A) is a U-shaped, tilted tube, 1.5–4 mm in diameter. The width increases towards top of the limbs. The trace fossil is 22 mm wide and up to 13 mm deep. *Arenicolites* Salter, 1857 is a dwelling and feeding burrow of suspension-feeding annelids (e.g. Hakes, 1976) or small crustaceans (Goldring, 1962). It occurs in facies of different environments, but is typical of shallow-marine settings (Crimes, 1977), especially in storm beds (Frey and Goldring, 1992).

Asterosoma (Fig. 10J) is visible in vertical section as oval spots, which are 14–18 mm thick. The spots are filled with slightly coarser material than in the surrounding rock. They may be in contact. The spots are interpreted as cross-sections of vertical to inclined elongated bulb-like structures tapering at both ends. They do not show concentric internal lamination typical of *Asterosoma* von Otto, 1854, but this is probably a matter of preservation. Clusters of such "bulbs" in *Asterosoma* form treelike structures spreading out from a common vertical or inclined shaft (e.g. Bromley and Uchman, 2003; Pervesler and Uchman, 2004). *Asterosoma* is interpreted as a selective-feeding burrow of a worm (Pemberton et al., 2001). It occurs in soft (mostly siliciclastic, rarely carbonate) substrates, typically in various shallow-marine settings, especially in the upper lower shoreface (Pemberton et al., 2001).

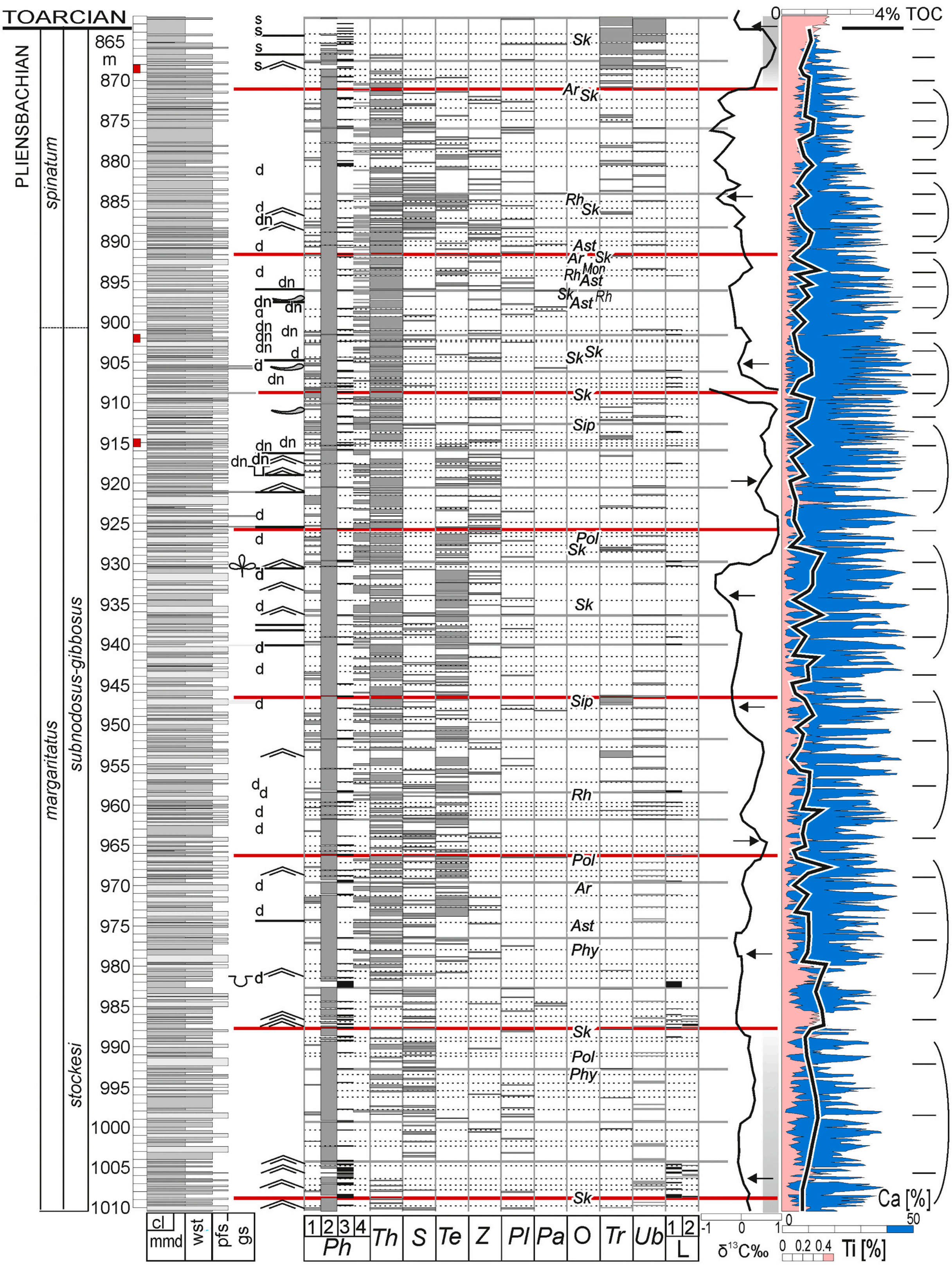

Fig. 4. Continuation of the Pliensbachian section in Mochras, depths are 1010.5–1123.8 m and 863.8–1010.5 m. Red squares in the depth columns – intervals presented in details in Figs. 5 and 6. For explanation see Fig. 3. (For interpretation of the references to colour in this figure legend, the reader is referred to the web version of this article.)

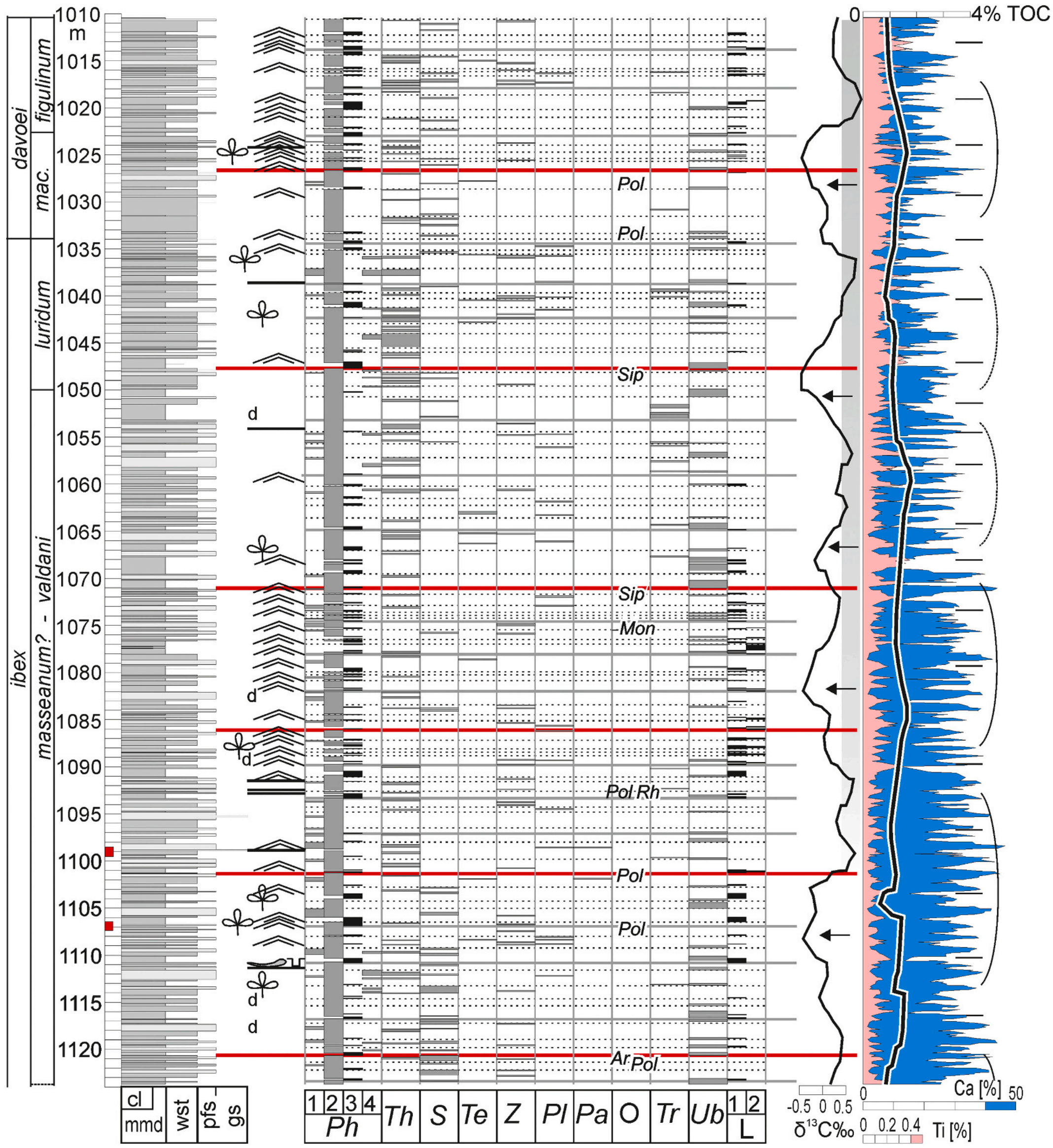

Fig. 4. (*continued*).

?*Monocraterion* is manifested on the vertical plane as a triangular structure, c. 10 mm wide and 10 mm high, with vertex oriented downward. This structure is interpreted as a cross section of a funnel at the top of a shaft. *Monocraterion* Torell, 1870 is a domichnial structure produced by suspension feeders (e.g. Westergård, 1931; Hallam and Swett, 1966; Pacześna, 1996; Jensen, 1997; Stachacz, 2016). For discussion of this ichnogenus see Jensen (1997) and Schlirf and Uchman (2005).

Phycosiphon incertum Fischer-Ooster, 1858 the most abundant trace fossil is a small structure, 1–15 mm wide, which comprises repeated narrow, U-shaped, irregularly branching lobes containing dark centres and light mantles. Dark tubes (centres) are composed of darker, finer sediment and are surrounded by a lighter mantle, composed of coarser sediment – see Figs. 8A–D, 9F, G, I, 10A, B, D, G, I, N). In places, dark centres show fish-hook shapes and pairs of black spots. The lobes are oriented randomly, although generally more or less parallel to bedding (however, parallel orientation may be also caused by compaction). Most commonly, *Phycosiphon* shows a diffused appearance due to soft-soupy host sediment and spreite structures and marginal tubes are very rarely observed – although their poor preservation seems to be generally typical for *Phycosiphon* (Wetzel and Bromley, 1994). The mantle and spreite indicate manipulation of grains, pointing to deposit-feeding activity. Four morphotypes of *P. incertum* can be distinguished: (1) the large Ph1 is 8–15 mm long, and 2–3 mm wide, (2) the medium, most common Ph2 is 3–8 mm long and 0.3–2 mm wide, (3) the small Ph3 is up of 2–3 mm long and 0.1–0.3 mm wide, usually horizontally oriented, and (4) Ph4 is distinguished by its occurrence in isolated patches; in this case, burrows similar to the morphotype Ph2 occur preferentially in fillings of *Thalassinoides* or occasionally in *Teichichnus*. The four morphotypes largely resemble these distinguished by Rodríguez-Tovar et al. (2014), although size of the morphotypes from the Mochras core are more diversified. Ph2 and Ph3 dominate. *Phycosiphon* is interpreted as the deposit-feeding trace of a small, unknown vermiform organisms that exploited the sediment for organic-rich matter (Wetzel and Bromley, 1994; Wetzel, 2010; Izumi, 2014); its morphological problems were studied by Naruse and Nifuku (2008) and Bednarz and McIlroy (2009). *Phycosiphon* is reported from a wide range of facies, but mostly from fine-grained lower shoreface and deeper, mainly siliciclastic deposits (Goldring et al., 1991; Savrda et al., 2001; Pemberton et al., 2012; Callow et al., 2013). Its tracemaker colonized freshly deposited turbidites in the sequential colonization model, when the sediment contained a lot of food and well oxygenated pore waters (Wetzel and Uchman, 2001). The *Phycosiphon* lobes can be inclined to varying degrees in the

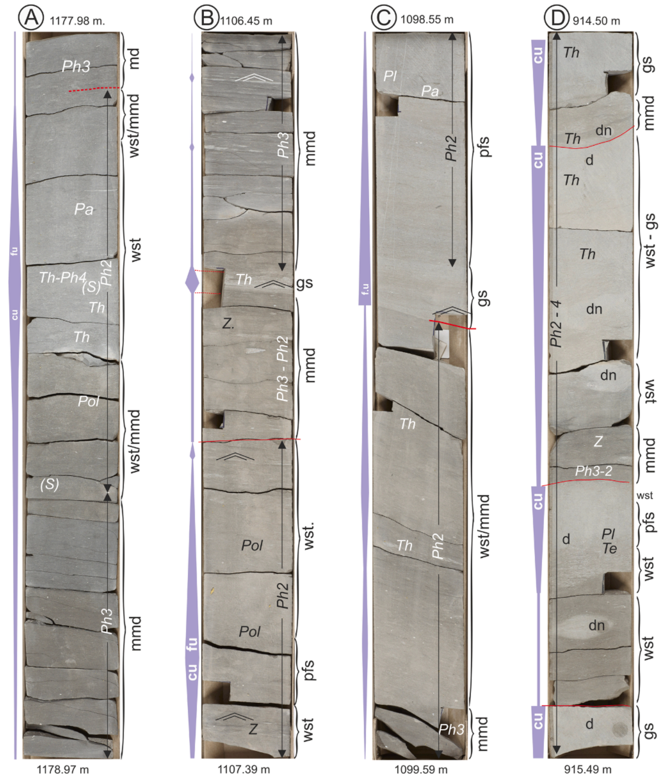

Fig. 5. Sections of the Mochras core showing common types of lithology, ichnology and cyclicity of sedimentation. A – 1177.98–1178.97 m: bigradational (symmetrical – cu – coarsening upward, fu – fining upward) cycle; m-md (micrite-calcareous mudstone) with *Phycosiphon incertum* type 3 is followed by muddy wackestone (w-st/m-md), wackestone (w-st) and subsequently again by mudstone – wackestone (w-st/m-md), all thoroughly bioturbated by *Phycosiphon incertum* type 2 (*Ph2*) makers, with appearances of the *Phycosiphon incertum* type 4 (*Ph4*) and sporadic *Schaubcylindrichnus*. This section is interpreted as a regular, C1-C2-C4-C5 contourite cycle with missing coarse division C3 (Stow and Faugères, 2008). The next cycle starts with mudstone (md) with *Phycosiphon incertum* type 3 (*Ph3*). *Phycosiphon incertum* obliterated primary sedimentary structures throughout the whole cycle, which points to well-oxygenated sea bottom. B – interval 1106.45–1107.39 m: bigradational cycle (cu – coarsening upward, fu – fining upward), starting and ending with mudstone/micrite and wackestone/siltstone facies with common *Phycosiphon incertum* type 2 (*Ph2*), in places with current structures; in the middle packstone-very fine grained sandstone (pfs) with *Phycosiphon incertum* type 2 (*Ph2*) and cf. *Polykladichnus* (*Pol*) dwelling structures. Next bigradational cycle (above cycle boundary – continuous red line) is built of fine-grained micrite/mudstone (m-md) parts separated by 5 cm-thick grainstone/sandstone intercalation with gradational boundaries and current structures (see Fig. 6.12); the upper "pinstripe" m-md interval contain thin, broken silty lamina and incipient ripples pointing to weak currents. The section 1106.45–1107.39 m is interpreted as two C1–5 contourite cycles (Stow et al., 2002). C – 1098.55–1099.59 m: bigradational cu-fu cycle showing subtle fluctuations in grain size (m-md – calcareous mudstone with *Phycosiphon incertum* type 3 – *Ph3*; w-st/m-md – wackestone/mudstone bioturbated by *Phycosiphon incertum* type 2 – *Ph2* makers, with rare occurrences of *Thalassinoides* – *Th*), topped by sharp erosional boundary with cross-bedded grainstone-sandstone (g-s) above, passing upwards into packstone - fine-grained sandstone (p-fs) with *Phycosiphon incertum* type 2 (*Ph2*), *Palaeophycus* (*Pa*) and *Planolites* (*Pl*). The upper cycle (g-s and p-fs) is interpreted as a base cut-out contourite C4–C5 – Stow and Faugères (2008). D – interval 914.50–915.49 m dominated by packstone and grainsyone with subordinate micrite/mudstone, showing stacked coarsening-upward cycles (red lines = cycle boundaries). Carbonaceous cementations (d) and carbonaceous nodules (dn) are common. This section is interpreted as stacked topcut-out contourite cycles C1-C2 (Stow and Faugères, 2008). For other abbreviations see Fig. 3. (For interpretation of the references to colour in this figure legend, the reader is referred to the web version of this article.)

sediment or horizontal orientation in laminated deposits; this pattern probably reflects the homogeneous distribution of food material or the concentration of food material in certain layers, respectively (Bromley, 1996).

Palaeophycus (Fig. 10C) is a sub-horizontal cylindrical, lined, passively filled burrow, 2–4 mm wide. It may show trace of collapsing. *Palaeophycus* Hall, 1847 is produced by variable filter or deposit-feeding, carnivorous or omnivorous invertebrates, mostly polychaetes in a wide range of facies (Pemberton and Frey, 1982; Jensen, 1997; Knaust, 2017).

?*Phymatoderma* (Fig. 9J,K) is a horizontal to subhorizontal structure composed of partly overlapping and diverging lobes, which are up to 6 m thick, 10–14 mm wide, and show crude spreiten. Pellets arranged perpendicular to the lobes, which are typical of *Phymatoderma* Brongniart, 1849 are not obvious (not preserved?). *Phymatoderma* is produced by deposit feeders which formed probes from a fixed position, which resulted in a fan-like structure (Fu, 1991; Uchman, 1999; Seilacher, 2007; Izumi, 2012).

Planolites (Fig. 8I) is a horizontal, unlined, cylindrical tunnel, actively filled with sediment usually differing from the surrounding. It is elliptical, sub-circular in cross sections, 2–3 mm in diameter. *Planolites* Nicholson, 1873 is an eurybathic, extremely facies-crossing ichnogenus referred to polyphyletic vermiform deposit-feeders producing active filling (e.g. Pemberton and Frey, 1982; Fillion and Pickerill, 1990, and references therein). Locklair and Savrda (1998) interpreted *Planolites* as an open burrow that was filled with overlying sediment. It can be abundant in deposits of well-oxygenated as well as in dysaerobic environments (Wignall, 1991, p. 268; Bromley, 1996).

cf. *Polykladichnus* (Fig. 10H) occurs in clusters, which are up to 20 mm wide and up to 20 mm high. It is composed of crowded, vertical to subvertical, branched, unlined cylinders, which are ~1 mm wide. The branches diverge in the middle-upper part under acute angle. *Polykladichnus* Fürsich, 1981 is a domichnion, which occurs mostly in marginal marine and continental deposits (Schlirf and Uchman, 2005). Burrows of such pattern are produced by some nereidid polychaetes (Wang et al., 2019).

Rhizocorallium (Fig. 10L) is visible in vertical section as 1) a dumbbell structure, about 60 mm wide, with lens-like, swelled terminations, which are 15 mm wide, and the interconnecting thin bar, which is 1.4–2 mm thick, or as 2) spreite horizontal structures, 5 cm thick with a swelling at the end. The lens-like terminations are interpreted as cross-section of marginal tunnels. *Rhizocorallium* is interpreted as a structure produced by suspension feeding (only short oblique, retrusive forms) or by deposit feeding organisms, mostly crustaceans (Fürsich, 1974; Schlirf, 2000) or "worms" (Knaust, 2013). Occurrences of *Rhizocorallium* are usually associated with occurrences of dwelling structures (*Skolithos*, *Arenicolites*,?*Monocraterion* or cf. *Polykladichnus*), sharp lithological boundaries and rare appearances of grainstone/sandstone (e.g. 1092.5 m – *ibex* Zone and 884.0–898 m interval in the *spinatum* Zone), which may indicate periods of slower sedimentation, stiffer ground and more vigorous currents. *Rhizocorallium* occurs mostly in shallow marine and marginal marine deposits (e.g. Farrow, 1966; Hakes, 1976) and rarely in deep-sea (Uchman, 1992) or even in non-marine deposits (Fürsich and Mayr, 1981).

Schaubcylindrichnus (Figs. 8 F, 9I) is usually represented by horizontal to oblique, single, simple tubes ~2–5 mm in diameter, rarely by a bunch of subparallel tubes, that display a white, calcareous/silty wall. No cross cuts by other trace fossils occur, which can be attributed to both deeper tier and reinforced walls. In most cases, this trace fossil occurs in fine-grained deposits (mudstone and wackestone). It is common in the lower *margaritatus* and the middle *spinatum* zones. *Schaubcylindrichnus* Frey and Howard, 1981 is interpreted as solitary funnel feeder and dwelling structure produced by enteropneusts, maldanid polychaetes or synaptid holothurians (Nara, 2006; Löwemark and Nara, 2013).

Siphonichnus (Fig. 9L) is a steeply inclined, simple tube, c. 1.5 mm thick, which shows a darker core and thick lighter mantle. In the upper part, it may show a swelling. *Siphonichnus* Stanistreet et al., 1980 is a

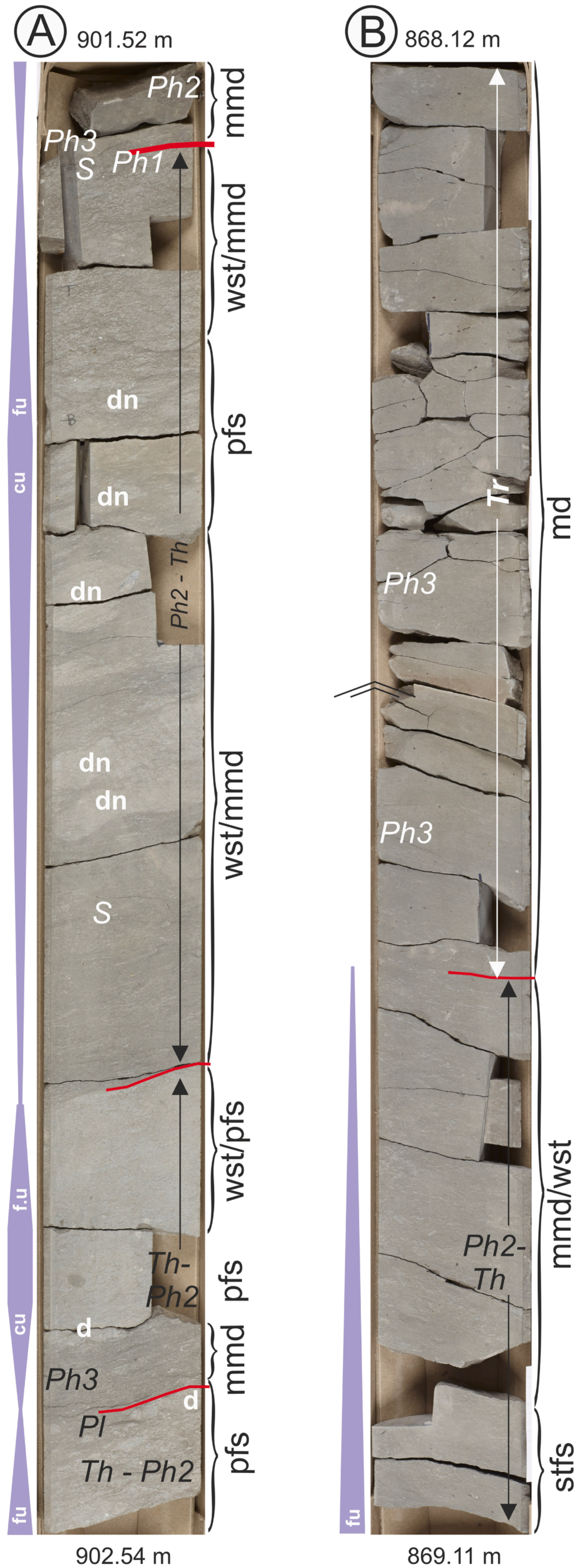

(caption on next column)

Fig. 6. Sections of the Mochras core showing common types of lithology, ichnology and cyclicity of sedimentation. A – 901.52-902.54 m – two bigradational cycles – the lower one is incomplete (condensed), topcut-out contourite cycle C1-C3 (Stow and Faugères, 2008). The upper cycle is of a more complete character, although lower mudstone part is missing. Note numerous carbonaceous nodules (dn). *S* = *Schaubcylindrichnus*. B – 868.12–869.11 m, uppermost Pliensbachian strata; end of the fining-upward, bioturbated cycle of contourite origin, topped by homogenous, structureless, "massive", non-calcareous mudstones with numerous *Trichichnus* (*Tr*) and very rare *Phycosiphon incertum* type 3 (Ph3). For other abbreviations see Fig. 3. This section is typical of "falling out of suspension" hemipelagic deposits – however, current structure in a thin silty intercalation points to intermittent current activity.

dwelling trace of suspension feeding bivalves (Stanistreet et al., 1980; Gingras et al., 2008; Dashtgard, 2011) or a pascichnion of bivalves such as tellinids (Knaust, 2015). It is commonly reported from shallow-marine and marginal-marine deposits (Pollard, 1988) often related to salinity fluctuations and freshwater influx (Knaust, 2015). Rarely, it is reported from deep-sea deposits (Krobicki et al., 2006).

Skolithos is visible as 1) isolated, vertical or steeply inclined, simple, unlined cylinder, ~ 1 mm wide, and at least 17 mm long, or as 2) isolated, vertical, slightly winding, tube ~1 mm wide and at least 30 mm long (Fig. 10D); the tube is lined with mud. *Skolithos* Haldeman, 1840 occurs in a broad variety of environments (Fillion and Pickerill, 1990 for review), but it is most typical of shallow-water-high energy settings, where it is interpreted as dwelling and feeding burrows of annelids or phoronids (Alpert, 1974). However, it may also occur in deep sea deposits (e.g. Wetzel, 2007).

Teichichnus (Figs. 8E, 9I, 10B) is a vertical, blade-like elongate spreite structure resulted from the upward or downward displacement of a causative tube. It is 15–25 mm wide and extends up to 60 mm in the vertical plane. In some examples, the vertical section shows zigzag margins typical of *Teichichnus zigzag* Frey and Bromley, 1985. Several specimens can be interpreted as incipient *Teichichnus*, because only a few spreiten laminae are developed in the basal part. *Teichichnus* is usually formed in a deeper tier than *Phycosiphon* and *Thalassinoides*, in slightly stiffer sediment. However, occasionally it is cut by Ph4 (Fig. 10B) and *Zoophycos*. It is particularly abundant in the *subnodosus* Subzone (Fig. 4). *Teichichnus* and *Schaubcylindrichnus* usually do not occur together. *Teichichnus* Seilacher, 1955 is a typical feeding structure. For discussion of this ichnogenus see Knaust (2017).

Thalassinoides (Figs. 8J, 9G, I, M, 10B) is visible in vertical section mostly as elliptical spots up to 5–20 mm wide, or short bars of comparable size, whose colour differs from the surrounding rock. Their sectioning reveals that they represent mostly horizontal, branched, cylindrical burrow networks. The vertical shafts connecting the system to the sediment surface are rarely preserved. The burrows are filled actively or passively. They are usually associated with coarser (packstone-grainstone), somewhat stiffer sediments. The filling is preferentially burrowed with *Phycosiphon*. In poorly cohesive sediments the burrow margins are diffuse. Other deformations may result from compaction or diagenetic dissolution of carbonate (cf. Archer et al., 1989). *Thalassinoides* cross cuts *Phycosiphon* of the morphotypes Ph1, Ph2 and Ph3, but is cut by Ph4, *Schaubcylindrichnus* and *Teichichnus*. Representatives of *Thalassinoides* Ehrenberg, 1944 occur in deposits of variable, presumably shallow marine environments (Frey et al., 1984; Mángano and Buatois, 1991; Pemberton et al., 2001), but also in the deep-sea facies (Uchman, 1995, 1998; de Graciansky et al., 1998; Uchman and Tchoumatchenco, 2003; Wetzel et al., 2007). They are produced mostly by scavenging and deposit-feeding crustaceans and interpreted as domichnia and fodinichnia (Frey et al., 1978; Frey et al., 1984; Bromley, 1996; Schlirf, 2000). For further discussion of this ichnogenus and its ichnotaxonomic problems see Fürsich (1973), Ekdale (1992) and Schlirf (2000).

Trichichnus (Figs. 8G, H, 10F) is a vertical to oblique, occasionally horizontal, straight or slightly winding, thread-like, unbranched or

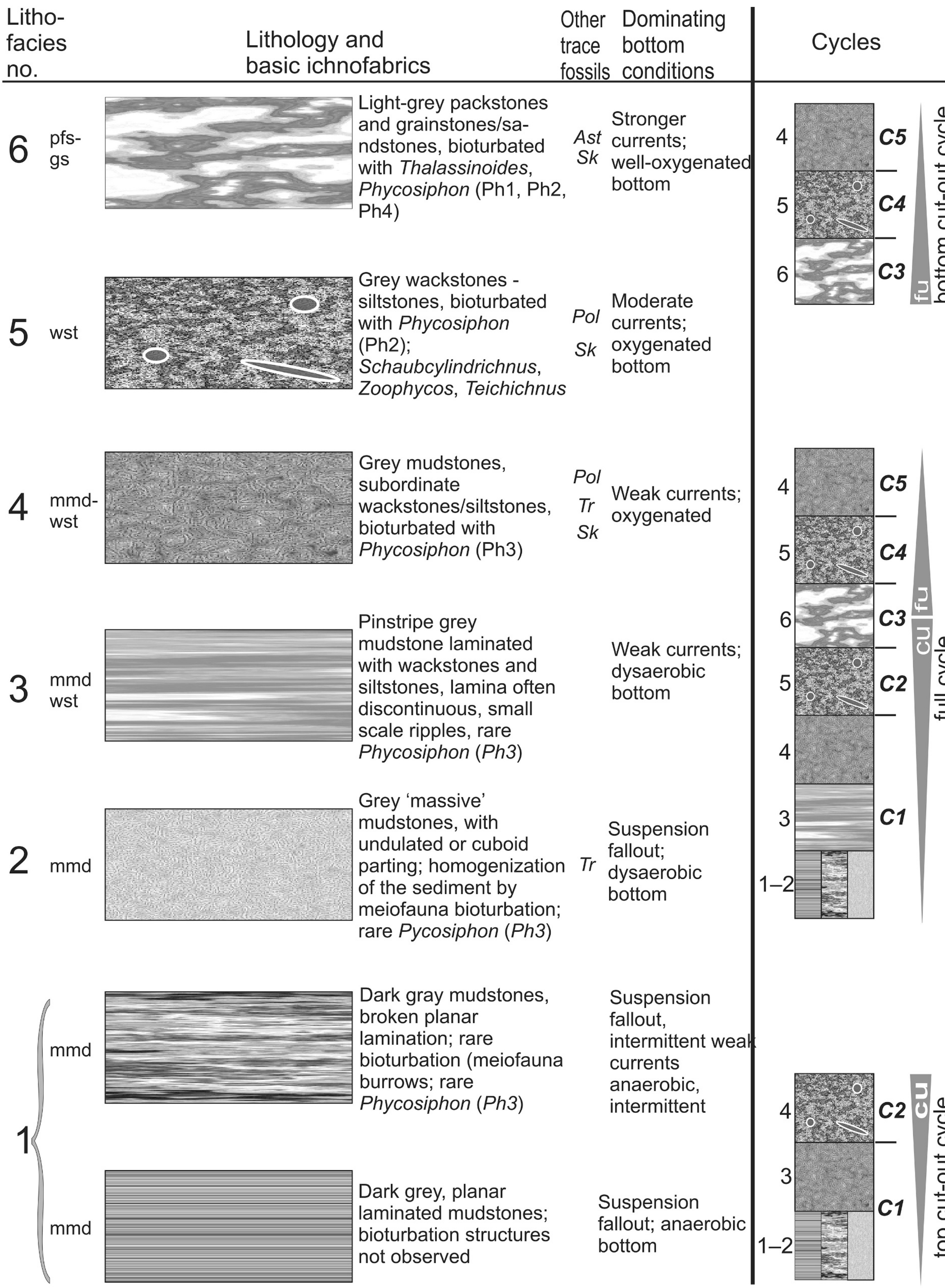

Fig. 7. Six main lithofacies (1–6) and ichnofabrics in the Mochras profile; to the right – main types of bigradational contourite drift sedimentary cycles built of main lithofacies – full cycle, top cut-out cycle, bottom cut-out cycle (referred to Stow et al., 2002; Stow and Faugères, 2008). Contourite cycle divisions reflect variations in current velocity. C1–C5 – "full" contourite cycle. For lithology and trace fossil abbreviation see Fig. 3.

branched cylindrical structure, up to 1 mm in diameter. It is an exceptional trace fossil due to its very small diameter (mostly less than 1 mm) and common pyritic filling. *Trichichnus* is particularly common in the uppermost *spinatum* Zone, which is associated with declining abundance in *Phycosiphon*, low ichnodiversity and specific clay mineral composition (Deconinck et al., 2019) pointing to a stressed environment. Modern analogues link *Trichichnus* Frey, 1970 to large, filamentous mat-forming, sulfide-oxidizing bacteria, belonging mostly to *Thioploca*-related taxa, which are able to house a complex bacterial consortium providing an electron exchange between oxic and suboxic/anoxic layers in the sediment (Kędzierski et al., 2015; Kjeldsen et al., 2019). *Trichichnus* occurs mostly in fine-grained sediments, in shallow water (e.g. Frey, 1970) as well as in deep-sea deposits (e.g. Kennedy, 1975; Wetzel, 1981, 1983). It is a deep-tier trace fossil having higher tolerance for dysoxia than *Chondrites* (Kotlarczyk and Uchman, 2012).

Zoophycos (Figs. 8J, 10I) is represented by a few mm thick, planar to oblique structures. The characteristic of *Zoophycos* spreiten structure is not observed, but this is common in some fine-grained deposits (Voigt and Häntzschel, 1956). *Zoophycos* is distributed rather evenly through the whole section, but rare in the lower *jamesoni* Zone and more frequent in the upper *margaritatus* to lower *spinatum* zones. Usually, only one, rarely two whorls appear (Figs. 8J, 10I). *Zoophycos* is not cut by other trace fossils. This indicates that it occupies the lowermost tier. *Zoophycos* Massalongo, 1855 is generally considered as a structure produced by some yet undiscovered deposit feeders, which are referred to as sipunculids (Wetzel and Werner, 1981), polychaete annelids, arthropods (Ekdale and Lewis, 1991), or echiuran worms (Kotake, 1992). The feeding strategy is, however, controversial (e.g. Bromley, 1991; Locklair and Savrda, 1998; MacEachern and Burton, 2000). Bromley and Uchman (2003) suggested that the upper helical part of a large Pliocene *Zoophycos* from Rhodes, Greece, is a deposit-feeding structure, and lateral lobes developing from its lower part are sulphide wells for chemo-symbiotic bacteria. Sediment of the spreiten derives from the sediment surface (Löwemark et al., 2006). Since the Mesozoic, *Zoophycos* has shown a tendency to occur in deeper environments than in the Palaeozoic, from below the shelf to abyssal depths (Zhang et al., 2015).

Trace fossil assemblages from the Mochras cores are strongly dominated by *Phycosiphon incertum*, which is the principal deposit-feeding trace. Other deposit-feeding traces, e.g. *Rhizocorallium* (Fig. 10L), ?*Phymatoderma* (Fig. 9J, K) and *Asterosoma* (Fig. 10J) are rare. Among other trace fossils, of note are occurrences of dwelling structures of filter-feeding organisms, building vertical structures stabilized by a mucus lining (*Skolithos*, ?*Monocraterion*, *Arenicolites*, *Siphonichnus*, cf. *Polykladichnus*).

All the described trace fossils are important components of ichnofabrics (ichnofabric is understood as an overall texture and structure formed by bioturbation or bioerosion; see Bromley and Ekdale, 1986). Constituents of ichnofabrics may be attributed to a number of controls and attributes, in particular to the tiering patterns and the manner of colonization (Ausich and Bottjer, 1982; Taylor et al., 2003). The complete ("ideal') tiering pattern in the Mochras section can be summarized as follows. The shallowest tier consists first of an indistinct mottling that is produced in the mixed layer by bioturbation in water-saturated soupy sediment near the sea floor, followed next by shallow tier of *Phycosiphon* (Ph1, Ph2, Ph3) showing a patchy distribution. In the middle tier, is *Thalassinoides* and bit deeper *Schaubcylindrichnus*, *Planolites*, rare *Teichichnus* and yet deeper another generation of *Phycosiphon* (Ph4), reworking *Thalassinoides* (and rarely *Teichichnus*) are present. The deepest tier is occupied by *Teichichnus* and *Zoophycos*. Rare traces (cf. *Polykladichnus, Skolithos, Arenicolites, Siphonichnus, Rhizocorallium,* ?*Phymatoderma*) usually occupy a middle tier, below *Phycosiphon* (Ph1, Ph2, Ph3). However, such a complete ("ideal") tiering pattern occurs rarely, and the most common tiering pattern is limited to shallowest tiers: *Phycosiphon* (Ph1, Ph2, Ph3), *Thalassinoides* (middle tier) and (less frequently) a bit deeper a *Schaubcylindrichnus* tier.

Thus, in most common ichnological cycles/colonization successions, *Phycosiphon* (Ph3, Ph2, Ph1) is followed by *Thalassinoides* (mostly in coarser sediments) and *Schaubcylindrichnus* (mostly in finer sediments). *Thalassinoides* is often burrowed with secondary, "patchy" Ph4, whose maker exploited more porous sediment of the burrow infill. Presence of more nutritious material within the *Thalassinoides* filling could be also considered. *Teichichnus* and *Zoophycos,* representing deeper tiers, are generally less common, except for in the mid-*margaritatus* Zone, where *Teichichnus* is very common, while *Zoophycos* is relatively more common in the *subnodosus-gibbosus* subzones to lower *spinatum* Zone. *Planolites*, *Palaeophycus* and other trace fossils occur sporadically.

In rare cases (e.g. lower *jamesoni* Zone, bottom of the *stokesi* Subzone, top of the *spinatum* Zone – the latter with domination of *Trichichnus* and scarcity or disappearance of other forms, including *Phycosiphon*), the impoverished tiering comprises from the bottom to the top: mottling or lamination-Ph3-Ph2-Ph1-Ph2-mottling; and in top cut-out cycles: mottling or lamination-Ph3-Ph2 (Fig. 7).

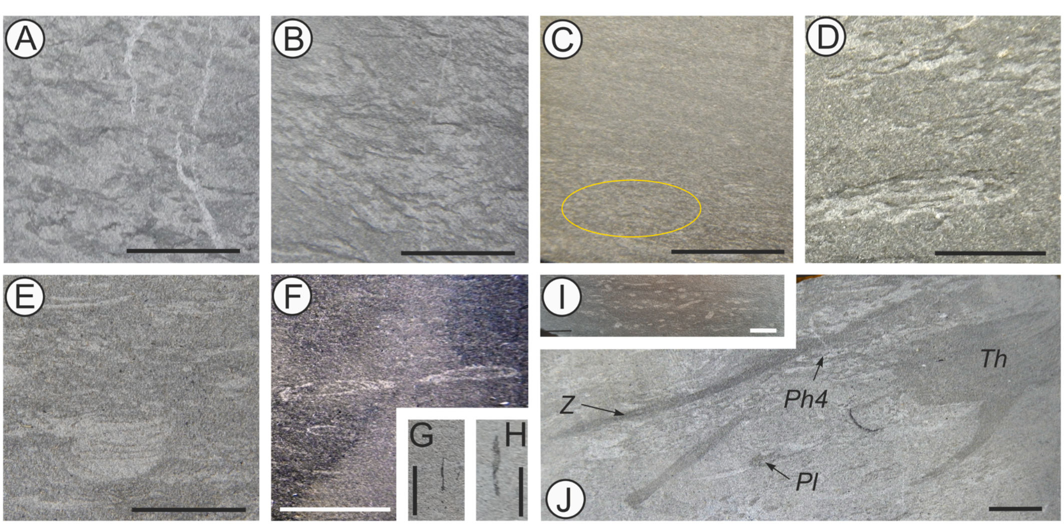

Fig. 8. Photographs showing most common trace fossils: A – *Phycosiphon incertum* morphotype 1 (*Ph1*), 1148.30 m; B – *Phycosiphon incertum* morphotype 2 (*Ph2*), 1145.0 m; C – *Phycosiphon incertum* morphotype 3 (*Ph3*), 1160.3 m; D – *Phycosiphon incertum* morphotype 4 (*Ph4*), 1158.90 m; E – *Teichichnus*, 934.85 m; F – *Schaubcylindrichnus*, 1011.20 m; G, H – *Trichichnus*, 947.10 m; I – *Planolites*, 988 m; J – *Thalassinoides* (*Th*), *Planolites* (*Pl*), *Phycosiphon* type 4 (*Ph4*) and *Zoophycos* (*Z*), 937.50 m. For more trace fossils examples see Figs. 9 and 10.

4. Discussion

4.1. Sedimentary environment, ichnodiversity, cyclicity of sedimentation

4.1.1. Sedimentary environment

On the basis of sediment transport processes, two different types of deep-water currents and their depositional products have been recognized and extensively documented in the literature, namely contourite drift facies produced by along-slope contour currents (Gong et al., 2017) and turbidite facies created predominantly by downslope sediment density flows. Turbidites are primarily bioturbated from the top (e.g. Uchman and Wetzel, 2011). The uppermost layers of the turbidite exhibit total bioturbation, which decreases with depth as lamination appears. In contrast, contourites typically exhibit a more continuous and uniform bioturbation, which appears throughout the entire contourite bed (Wetzel et al., 2008). It should be noted, that turbidites can be reworked by contourite currents. Recently, de Castro et al. (2020a) described a Quaternary case of mixed deposits, called "bottom current reworked sands" (BCRS). The sequence is defined as a partial bi-gradational contourite sequence including BCRS reworked from underlying turbiditic deposits due to the interaction of down- and along- slope processes within the contouritic drift and its adjacent contouritic channel. As a result, the contourite drift and the adjacent contourite channel are influenced by the interrelation of hemipelagic, gravitational, and bottom current induced depositional processes (de Castro et al., 2020b). Rodríguez-Tovar et al. (2019) showed an Oligocene-Miocene example with a more complex internal pattern of contourites, characterized by a more discontinuous, multiphase sedimentation, resulting also in ichnological differences between non-compacted and compacted interlayers. However, in Mochras such differentiation in compaction of trace fossils is not observed. Also, sandstone and grainstone or erosional features are very rare, while even distal turbidite deposits, hyperpycnites and BCRS or other mixed contourite-turbidite deposits contain appreciable sand and are dominated by numerous erosional features and variable scale cross-bedding which result from more or less instantaneous deposition (Etienne et al., 2014; Rodríguez-Tovar et al., 2019; de Castro et al., 2020a, 2020b). Moreover, rare sandy beds and laminae in Mochras show no systematic vertical grading and

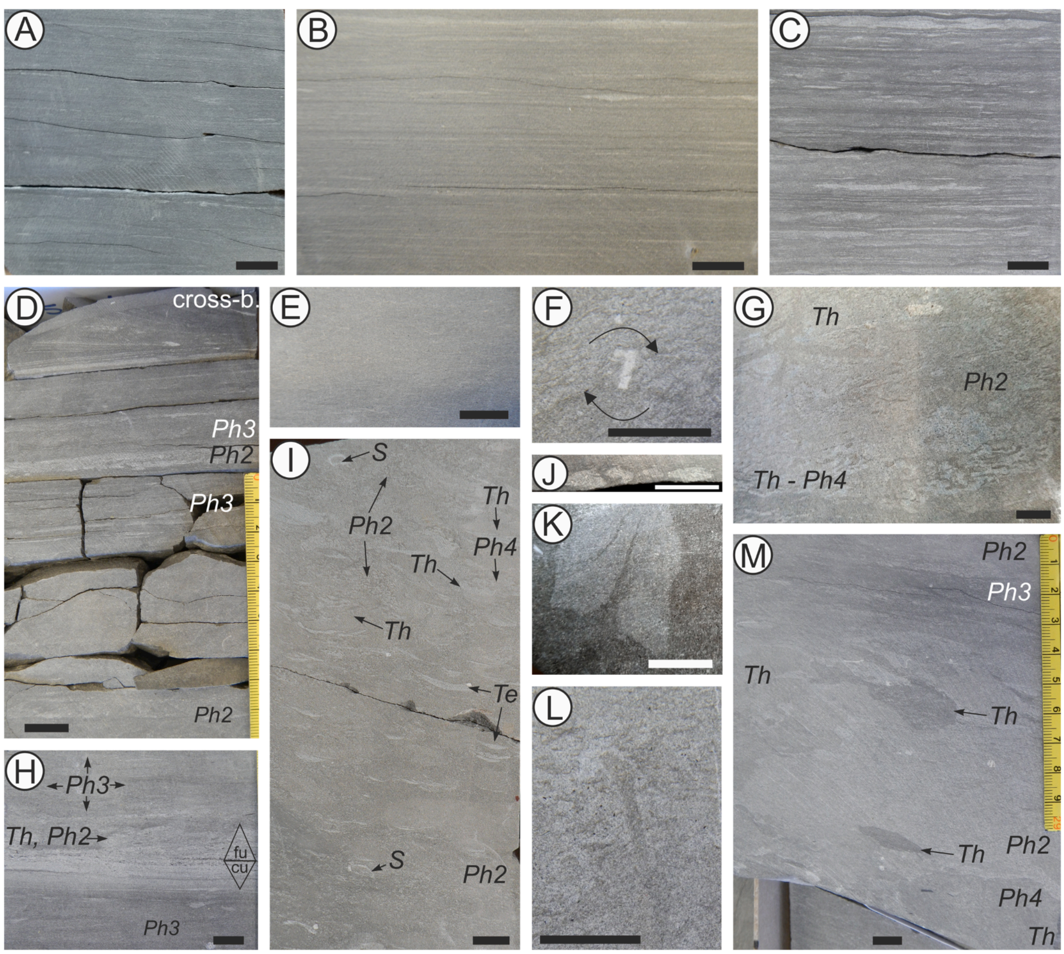

Fig. 9. Some sedimentary and ichnological features. A – continuous planar lamination in mudstone, 1233.5 m; B – continuous planar lamination passing upwards into broken lamination with incipient ripples indicating weak currents, 1077.2–1077.3 m; C – "pinstripe" broken lamination, in places continuous, showing silty/calcareous lamina and ripples produced by currents, 1005.5–1005.6 m; D – succession showing "massive" mudstone with *Phycosiphon* morphotype 2 (*Ph2*) passing upwards into "pinstripe" mudstone laminated with calcareous siltstone with *Phycosiphon* morphotype 2 and 3 (*Ph2* and *Ph3*) and subsequently into cross-bedded wackestone at the top, indicating increasing current activity, 1071.65 m; E – "massive" mudstone, result of meiofauna bioturbation, 1123.1 m; F – crinoid rotated by burrowing activity of *Phycosiphon incertum* makers, which points to soft-soupy ground conditions, 1098.35 m; G – *Thalassinoides* (*Th*), in the bottom filled with *Phycosiphon incertum* type 4 (*Ph4*), earlier *Phycosiphon incertum* morphotype 2 (*Ph2*) in the background, 888.25 m; H – grainstone/sandstone intercalation with gradational lower and upper contacts (cu – coarsening upward, fu – fining upward) and low-angle cross bedding; fragment of the Fig. 5.2, depth 1106.8 m; I – ichnofabric showing succession of the earliest/shallowest tier *Phycosiphon incertum* morphotype 2 (*Ph2*), followed by *Thalassinoides* (*Th*), *Schaubcylindrichnus* (*S*) and *Teichichnus* (*Te*). Note *Phycosiphon incertum* morphotype 4 (*Ph4*) reworking (postdating) *Thalassinoides*, 973.25–973.45 m; J – feeding burrow ?*Phymatoderma*, cross-section, 978.2 m; K – plane view of the?*Phymatoderma* shown above, 978.2 m; L – *Siphonichnus*, 913.1 m; M – *Thalassinoides* and *Phycosiphon* (*Ph3* and *Ph2* predating, *Ph4* postdating *Thalassinoides*), 1069.8 m.

stacking of structures such as those recognized in the Bouma (1962) turbidite intervals or those occurring in some sandy contourites (Rodríguez-Tovar et al., 2019). Instead, the Pliensbachian section in Mochras records continuous sedimentation controlled by fluctuation of stable and generally weak bottom currents; thus intermittent deposition by distal turbidite/hyperpycnite or BCRS was unlikely and the traditional contourite drift model (dominated by muddy sediments) fits the Mochras case - perhaps, with a few exceptions mentioned above (occurrences of *Rhizocorallium* and more frequent dwelling structures, more common sharp lithological boundaries and appearances of grainstone/sandstone, which may indicate periods of slower sedimentation, stiffer ground and more vigorous currents at 1092.5 m (*ibex* Zone) and between 884.0 and 898 m (*spinatum* Zone).

The lithofacies in the Pliensbachian at Mochras also contrast with those of other hemipelagic settings of the UK Jurassic. For example, the Pliensbachian in the Cleveland Basin, some 300 km to the NE of Cardigan Bay, is clearly dominated by structures attributable to storm processes in offshore shelf to shoreface environments (e.g. van Buchem and McCave, 1989; Van Buchem et al., 1994; Hesselbo and Jenkyns, 1995; Van Buchem and Knox, 1998; de Graciansky et al., 1998; Powell, 2010). Evidence of storm-influenced deposition in the Cleveland Basin includes winnowed shell beds and scours, symmetrical ripple structures, and ultimately in the sandy facies hummocky cross stratification. None of these diagnostically storm generated features has been observed in the Mochras Pliensbachian.

The contourites in Mochras can be classified as mixed calcareous

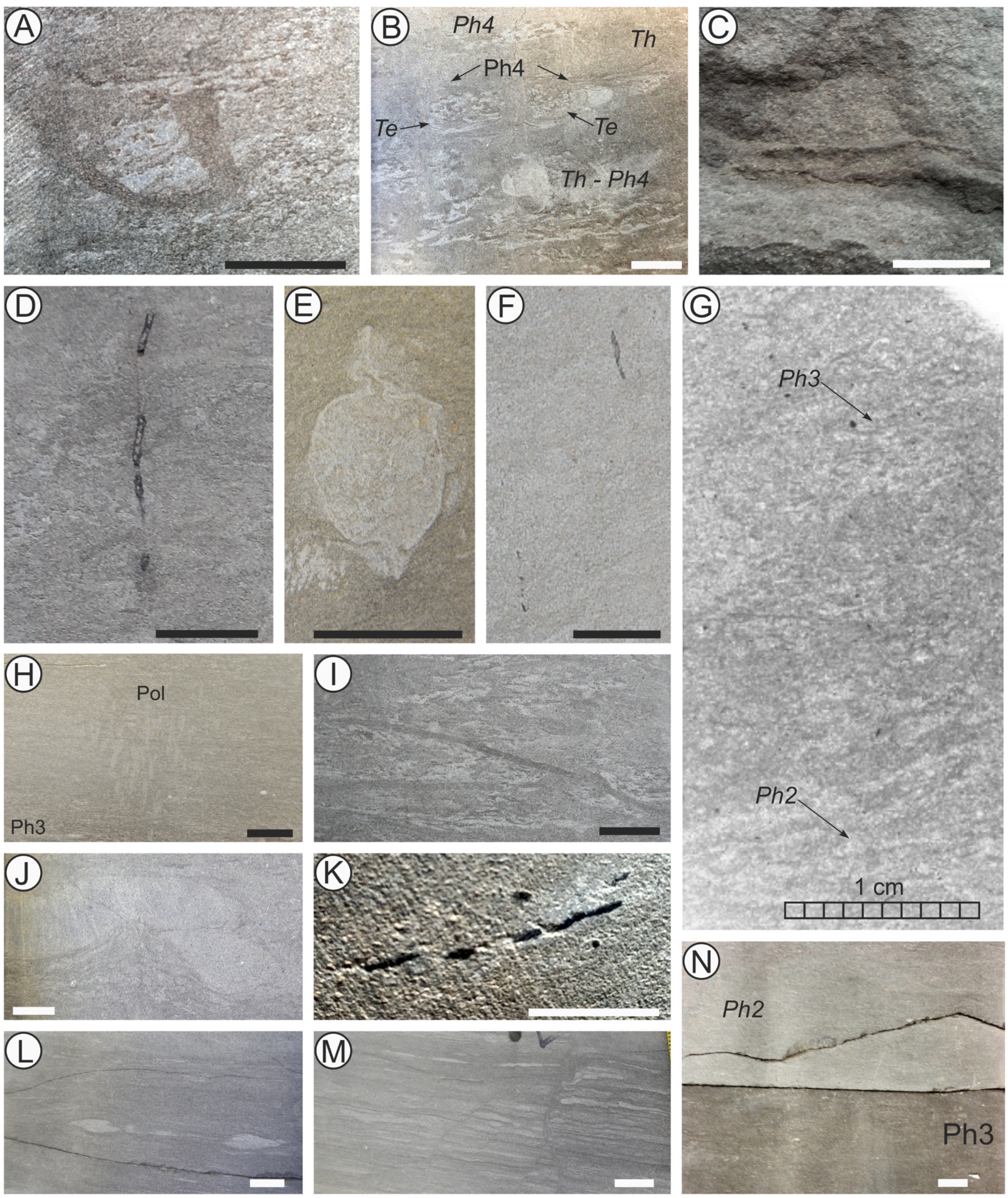

Fig. 10. Trace fossils in the investigated interval of the Mochras Borehole. A – dwelling burrow *Arenicolites*, 970.5 m; B – secondary *Phycosiphon incertum* (*Ph4*) partly reworking *Thalassinoides* (*Th*) and *Teichichnus* (*Te*), 1169.1 m; C – *Palaeophycus*, plane view, 984.7 m; D – dwelling burrow *Skolithos*, 886.2 m; E – bivalve buried in life position, 1131.6 m; F – *Trichichnus*, 947 m; G – thin section showing two *Phycosiphon incertum* morphotypes: *Ph3* and *Ph2*, 961.3 m; H – cf. *Polykladichnus* dwelling structure (*Pol*), *Phycosiphon incertum* morphotype 3 (*Ph3*) in the background, 1160.3 m; I – *Zoophycos* crosscutting *Phycosiphon incertum* morphotype 2, 926 m; J – *Asterosoma*, 917.5 m; K – "pyritized tube", 868 m; L – *Rhizocorallium*, 1092.75 m; M – dehydration cracks, 1024.9 m; N – sharp erosional boundary between mudstone and overlying grainstone, 1009.7 m. All scales = 1 cm.

Table 1
Comparison of the Walsh power-spectrum periodicities recognized from the occurrences of trace fossils with the orbitally-forced periodicities calculated by Berger (1977).

Phycosiphon morphotype 1 [kyr]	*Phycosiphon* morphotype 3 [kyr]	*Phycosiphon* morphotype 4 [kyr]	*Schaubcylindrichnus* [kyr]	*Thalassinoides* [kyr]	Lamination [kyr]	Orbital cycles [kyr] after Berger (1977)	
		115.4				112	Eccentricity bands
~100			94.4	114	94.4	95	
		64.9				59–64	Combined effect
54.6	54.6					54	Obliquity bands
40.7	42.4	42.4	41.5	39.2	40.7	40–42	
28.9	29.2	28.9		31.9	28.9	29–30	
22	23.3	24.4			20.6	22–24	Precessional bands
19	19	18.5	19	17.6		19	
			17	14.4; 15.5	16.4	16–17	

Table 2
Relative sedimentation rate (based on ichnology), number and average duration of 4th order (precession) cycles, number of 3rd and 2nd order cycles in the Pliensbachian stage of the Mochras core. Note fluctuation of average duration of 4th order cycles.

Stage	Ammonite Zone	Thickness (m)	Relative duration – based on ichnology (Myr)	Sedimen-tation rate -cm/1000 years	Number of 4th order cycles (precession-dominated)	Average duration of 4th order cycle	Number of 3rd order cycles (short excentricity – 100 kya)	Number of 2rd order cycles (long excentricity – 400 kya)
Pliensbachian – **387 m**	*spinatum*	**37**	0.8	4.6 cm/1kyr	31	25.8 kyr	8	2
	margaritatus	**110**	2.33	4.7 cm/1kyr	103	22.3 kyr	23.3	5.5
	davoei	**24**	0.47	5,1 cm/1kyr	23	21.7 kyr	4.7	1.2
	ibex	**90**	2.0	4.5 cm/1kyr	85	23.5 kyr	20	4.7
	jamesoni	**126**	2.8	4.5 cm/1kyr	113	24.8 kyr	28	6.7

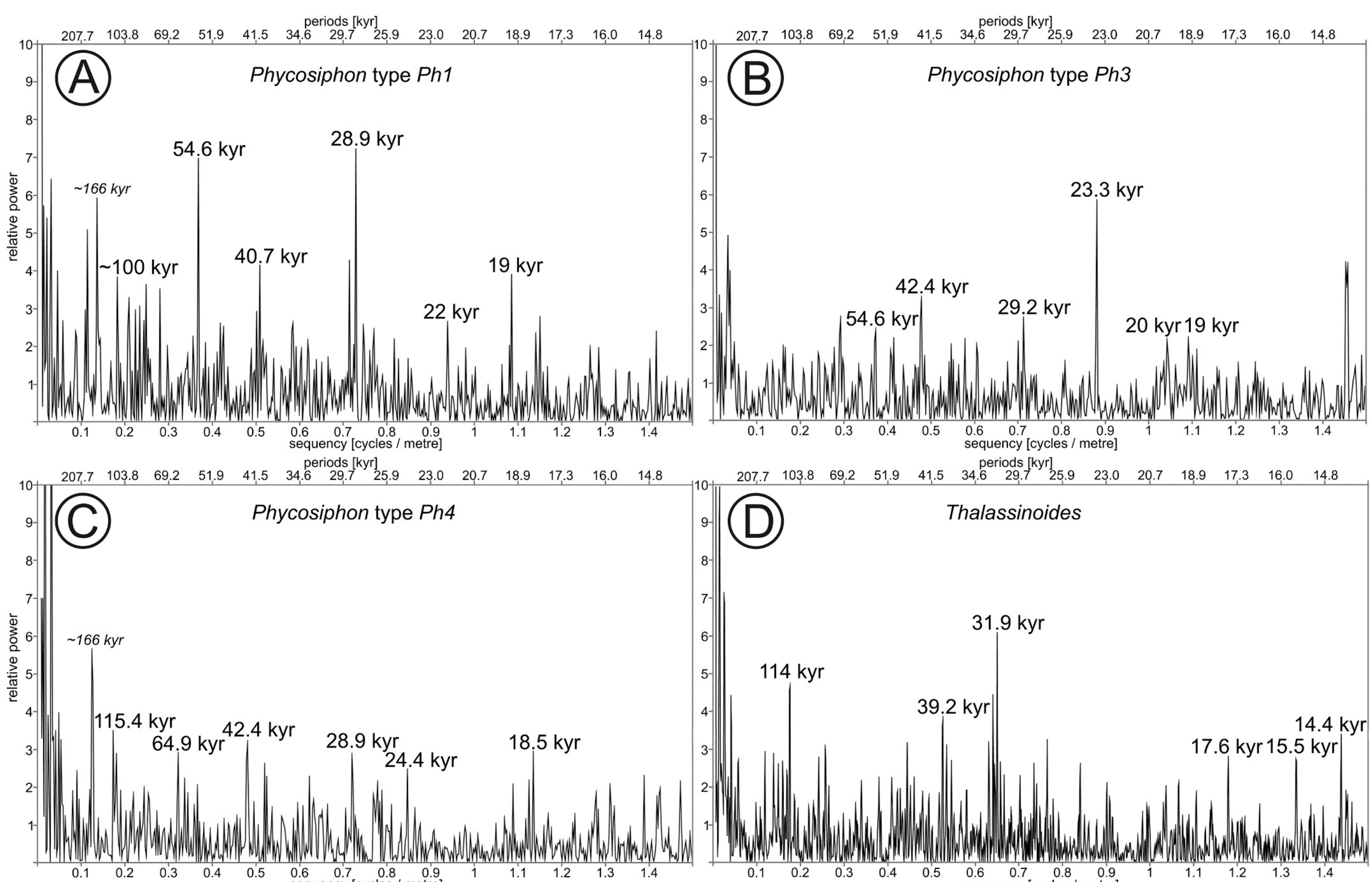

Fig. 11. Walsh power-spectra of the time series based on occurrences of respective trace fossils: A – *Phycosiphon* morphotype *Ph1*; B – *Phycosiphon* morphotype *Ph3*; C – *Phycosiphon* morphotype *Ph4*; D – *Thalassinoides.*

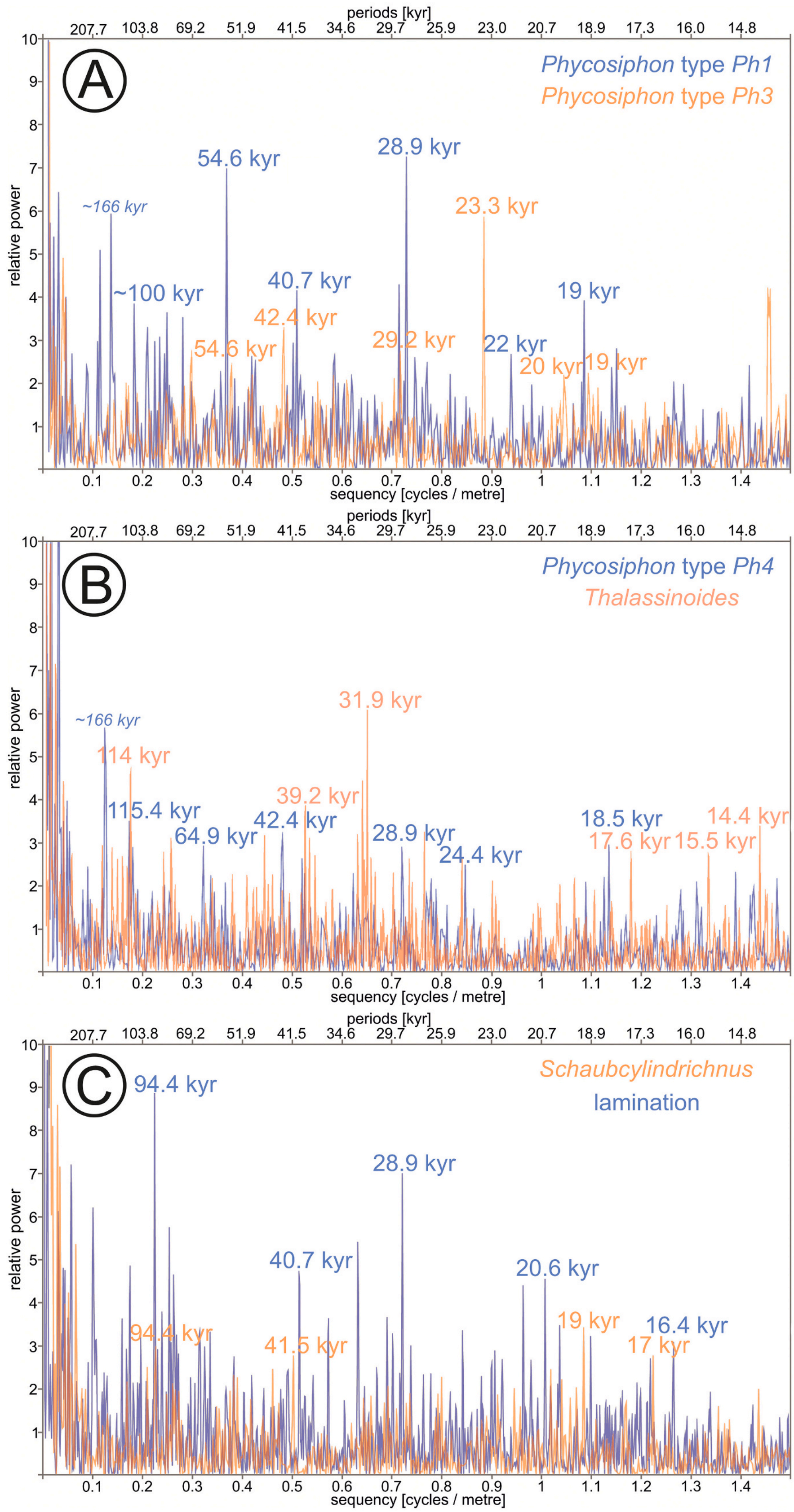

Fig. 12. Overlapping Walsh power-spectra of the time series based on occurrences of respective trace fossils and lamination: A – *Phycosiphon* morphotype *Ph1* and *Ph3*; B – *Phycosiphon* type *Ph4* and *Thalassinoides*; C – *Schaubcylindrichnus* and lamination.

biogenic-clastic contourites, the most frequent contourite facies in the modern oceans (Fagueres and Mulder, 2011). Hemipelagic mudstone, wackestone/siltstone and coarser packstone and grainstone of the Mochras section are usually poorly sorted or impure and appear to be structureless or mottled. The mottling results from intense bioturbation driven by the organic-matter supply from bottom currents (see Miguez-Salas et al., 2020 for a Miocene example). However, in less strongly bioturbated sections primary sedimentary structures are visible and they are mostly represented by current structures such as planar parallel lamination, low angle cross-lamination, starved ripples, in places subtle erosive bases, and gradational (rarely sharp) normal- and inverse-grading bed transitions, similar to cases studied by Shanmugam (2000) and Knapp et al. (2017). Stagnant conditions or very slow currents are interpreted to have allowed vertical settling of the suspended particles from the nepheloid layer (Ewing and Thorndike, 1965; Mulder et al., 2003), producing mottled mudstone (Figs. 3B2, 9E) or laminated mudstone-claystone (Figs. 3B1, 9A, B), where the grain-supported laminae are interpreted to be the result of very weak contour currents that winnowed out clay-sized sediment (e.g. Shanmugam, 2000). Periodically higher bottom-current velocities led to deposition of silt or sand layers with planar or low-angle cross-bedding, produced by bedload transport (Figs. 5B, C, 9C, D, H). The concentrations of plant remains – a feature particularly of the Pliensbachian in Mochras (Ullmann et al., 2021) – indicates phytodetrital pulses in connection with fluvial discharges in the vegetated hinterland. Relatively weaker bioturbation can be attributed to oxygen depletion or high sedimentation rate (Stow and Faugères, 2008). Stronger bottom currents also do not favour preservation of biogenic structures (Tucholke et al., 1985).

Fully developed bigradational intervals in the Mochras section (Figs. 3B, 5A, B, 7) correspond to a standard contourite sequence (Faugères et al., 1984; Stow and Holbrook, 1984; Stow et al., 2002; Faugères and Stow, 2008; Hüneke and Stow, 2008; Mulder, 2011; Rodríguez-Tovar and Hernández-Molina, 2018). The standard model was enhanced by introduction of interval divisions (C1 to C5; Stow et al., 2002; Stow and Faugères, 2008, their Fig. 13.9) and recognition of variations within partial contourite sequences (Rebesco et al., 2014; Shanmugam, 2017), corresponding to observations in the Mochras profile (Figs. 3B, 5–7) where most frequent vertical sequences consists of lithofacies types 1/2–3–4-5-6 (in coarsening-upward order) and subsequent fining-upwards couplet composed of 5–4 lithofacies types. The fining-upward phase of the fully developed cycle is usually thinner and incomplete (Figs. 3B, 5A–C, 7).

Additionally, observed types of more or less complete cycles were controlled by fluctuating sedimentation rate and, to a lesser extent, by carbonate dissolution, calcite replacement and cementation processes (Figs. 5D, 6A) at early diagenetic stage, possibly resulting from the degradation of organic matter and the associated reduction of sulphate, as evidenced by the occurrence of pyrite framboids (Ruhl et al., 2016). Periods of stronger currents marked by sharp surfaces (Fig. 10N) and coarser material such as shell debris are rare, occurring mostly between 900 and 940 m (*gibbosus* Subzone). In such cases the bigradational grading cycles are often incomplete, lacking upper parts (top-cut-out cycles; see Figs. 5D, 7) or lower parts (base-cut-out cycles; see Figs. 5C, 7, 10N).

4.1.2. Ichnodiversity

Appearances of trace fossils show cyclic character, more or less corresponding with lithological changes and sedimentary cycles. Diffused shape of trace fossils indices of soft-bottom condition (Fig. 9F), and domination of opportunist, r-selected *Phycosiphon*, mostly simple tiering, scarcity of highly-specialized, K-selected forms, all indicate generally high sedimentation rate associated with instability of substrate and benthic food availability (delivered either by currents or suspension fallout), interrupted by interim oxygen-depleted, more stagnant conditions – usually associated with darker sediments and lamination. The other end of the spectrum is characterized by higher substrate stability (stiffer conditions), diminishing sedimentation rate, continuous delivery of suspended nutrients by currents, and better bottom oxygenation leading to a more complex tiering under equilibria (Taylor et al., 2003). A high degree of bioturbation (Figs. 3B, 5A, D, 6A, 9F, I, L, M) is characteristic for contourites due to additional food supply and faunal abundance (Wetzel et al., 2008). In agreement with Caswell and Frid (2017), changes in community composition are usually linked to local redox conditions, whereas changes in populations of r-selected opportunists are driven by primary productivity. Because suspended organic matter is often adsorbed onto suspended clay minerals (Mayer, 1994), contour currents supply food to deep-marine benthic organisms (Thistle et al., 1985). If the vertical particle flux is supplemented by lateral current-carried supply, the benthos exhibits a higher biomass, population density, and resulting degree of bioturbation than on adjacent tranquil sea-floor fuelled only by a vertical flux of organic matter that decreases exponentially with water depth (Suess, 1980; Wetzel et al., 2008). As the whole Pliensbachian section is strongly dominated by *Phycosiphon* (Ph2), any lack of this morphotype is noteworthy as it indicates relatively rare, exceptionally unfavourable conditions, most likely associated with intermittent more stagnant conditions and oxygen depletion (occurring more frequently only in a few intervals: Sinemurian–Pliensbachian transition (lowermost *jamesoni* Zone), the mid-*ibex* Zone, the lower *stokesi* Subzone and the Pliensbachian–Toarcian transitional interval (uppermost *spinatum* Zone). Commonly, in such sections *Phycosiphon* (Ph3) appears (colonization after meiofauna mottling) as the first recognizable trace fossil, before Ph2 and Ph1 return.

4.1.3. Cyclicity of sedimentation

Distinction of cycles identified in this paper is based mainly on grain size and ichnological features and their lower boundaries are placed in the fine-grained, mottled or laminated micritic mudstone (lithofacies 1 and 2; see Fig. 7). Primary sedimentary structures are commonly obliterated by bioturbation, so these play a subordinate role in determining sedimentary cycles.

Both the fully-developed (bigradational), and the incomplete lithological couplets with their ichnological content, constitute the 4th order cycles, basic "building blocks" of the hierarchical order of cycles in Mochras. These 4th order cycles are arranged in higher hierarchical successions, usually containing four 4th order cycles.

The higher, 3rd order, cycles have different appearance depending on their position in the profile: in the *jamesoni* to lower *ibex* Zone and lower *margaritatus* (lower *stokesi* Subzone) they usually start with lamination and end with denser *Schaubcylindrichnus*, while in the upper *ibex* and *davoei* zones, the upper *margaritatus* Zone (*subnodosus-gibbosus* sub-zones) and *spinatum* Zone, they often start with *Phycosiphon* (Ph3) and end with denser *Thalassinoides* (in the uppermost *spinatum* Zone also *Trichichnus*). In some cases, larger deposit feeder structures (?*Phymatoderma*, *Rhizocorallium*) or dwelling/suspension feeders' structures (*Siphonichnus, Arenicolites, Skolithos*) appear in the upper parts of these cycles, interestingly in a few cases also in intervals indicating features of oxygen depletion in sediment (e.g. lamination at the depth 1245 m). This observation probably points to an episodic delivery of oxygen to the bottom waters (likely by currents) that allowed temporary development of bottom-dwelling fauna. With respect to behavioural groups, suspension feeders are not abundant, probably as their filter apparatus can easily be plugged when the mineral suspension concentration is high (Pieńkowski, 1985; Thistle et al., 1991).

The next in hierarchy are 2nd order cycles, composed of four 3rd order cycles – in most cases upper boundaries of these cycles are marked by the dwelling structures cf. *Polykladichnus* (in 9 cases) or by *Skolithos*, *Arenicolites*, *Siphonichnus* (11 cases), which characterise 20 of 21, 2nd order Pliensbachian cycles. Tops of the 2nd order cycles are marked also by increased (in relation to neighbouring beds) $CaCO_3$ content (Figs. 1, 2). In the Mesozoic, periods of maximal eccentricity are often associated with annually dry climates, disturbed by short periods of intensive summer rainfalls and storms, alternately in the Northern Hemisphere and the Southern Hemisphere (Boulila et al., 2011; Martinez and Dera, 2015), which translated into oceanographic circulation and observed ichnological changes and appearances of dwelling structures. The 2nd order (long eccentricity) cycles of 405 kyr duration are considered as stable over hundreds of million years (Kent et al., 2018).

The longest, 1st order cycles are characterized by more general changes – the most visible is ichnodiversity and abundance of trace fossils, which increase in two longer sections, in the higher *jamesoni* to lowermost *ibex* Zone, and then particularly in the middle *margaritatus* to lower *spinatum* zones. Recurrent higher ichnodiversity (excluding *Trichichnus*) is not associated with frequency of current structures (and bottom oxygenation), grain size or TOC content (Figs. 1, 2), but with higher content of $CaCO_3$ in relation to siliciclastic clay mineral component (Figs. 1, 2; Ruhl et al., 2016). Interestingly, higher ichnodiversity is also associated with clay mineral composition (Deconinck et al., 2019), namely with higher content of smectite and mixed layer (smectite/illite) clay minerals, while sections enriched in kaolinite generally show (besides lower abundance of trace fossils and more common lamination) a lower ichnodiversity. The relationship may be explained by the influence of expandable clay minerals (smectite and smectite/illite) on reduction of pore space and in consequence limitation (although not elimination) of the *Phycosiphon* trace makers, which are dependent on oxygen acquired from pore water. Only with limited competition from the *Phycosiphon* trace makers could other trace makers develop in a higher diversity and quantity. The 1st order cycles are divided by intervals showing oxygen depletion in bottom sediment (registered also by HI index; see Storm et al., 2020), more frequent appearances of lamination, carbonate depletion, oxygen deficiency resulting in *Phycosiphon* crises, and numerous occurrences of *Trichichnus* representing filamentous mat-forming, sulphide-oxidizing bacteria. Such intervals appeared four times: in the Sinemurian–Pliensbachian transition zone, the mid-*ibex* Zone, the upper *stokesi* Subzone (c. 985 m), and at the Pliensbachian–Toarcian transition, although the latter level is distinctive with a domination of *Trichichnus* and poor diversity in benthic foraminiferal morphogroups, dominated by opportunist epifaunal forms of the genus *Reinholdella* (Rodríguez-Tovar et al., 2020). The topmost Pliensbachian section is characterized by abundance of mixed layer clay minerals and presence of berthierine, which has been attributed by Deconinck et al. (2019) to sea-level fall, climate cooling and enhanced physical weathering on the land, although according to Ruebsam et al. (2020), the Pliensbachian-Toarcian transition was characterized rather by elevated temperatures. Although bottom-life crises at the 1st order cycle boundaries occurred four times in Pliensbachian as described in the present study, the Pliensbachian-Toarcian crisis was exceptional in its severity and continued to the earliest Toarcian (Dera et al., 2011; Xu et al., 2018). Most likely, the benthic crisis was connected with general, exceptional stagnation of circulation through the Laurasian Seaway (and the Cardigan Bay Strait) at that time (Van de Schootbrugge et al., 2019).

The major clayey, carbonate-free or carbonate-depleted intervals with marked *Phycosiphon* crises (oxygen depletion) record major sedimentary changes, which seem to occur in a long-term, but approximately regular manner. Oxygen deficiency can be attributed to diminishing current intensity, but also to number of other related or independent causes, including sea-level, acidification of oceans and dissolution of $CaCO_3$ related to carbon cycle (e.g. Lord et al., 2016). According to Ayranci et al. (2018), highstand and transgressive systems tracts in contourites are both represented by dominantly massive mudstone lithofacies, sparse bioturbation and higher TOC values. Such features (or at least two of them) occur in the Sinemurian–Pliensbachian transitional section, the mid-*ibex* Zone, the lower *stokesi* Subzone and the Pliensbachian–Toarcian transitional section (Figs. 1, 2). However, the mid-*ibex* Zone retains significant $CaCO_3$ content and the lower *stokesi* Subzone and the upper *spinatum* Zone are associated with regressions and relative sea-level fall in UK (de Graciansky et al., 1998; Hesselbo, 2008; Deconinck et al., 2019). Thus, changes in oceanic circulation, connected with major climate and carbon cycle changes, would be a more likely scenario than sea-level rises. Sea-level rise could possibly be a significant additional factor in the beginning of Pliensbachian, as the marked sea-level rise is widespread and documented not only in UK, but also in Germany, Poland and Scandinavia (Sellwood, 1972; de Graciansky et al., 1998; Hesselbo, 2008; Pieńkowski, 2004; Barth et al., 2018).

The results obtained allow interpretation of palaeoceanographic circulation in Pliensbachian times. According to Shanmugam (2017), the facies term "contourite" is appropriate only for deposits of thermohaline-driven geostrophic contour currents in deep-water environments. However, according to other authors, a wide spectrum can be expected, as such currents are not confined to a deep sea and have been associated with either deep (e.g. Borisov et al., 2013; Martos et al., 2013), intermediate (e.g. Bein and Weiler, 1976; Van Rooij et al., 2010; Rebesco et al., 2013) or shallow (epicontinental) water masses (e.g. Vandorpe et al., 2011). Calcareous deposits (loosely chalks) from the North Sea region (for the Late Cretaceous case) suggest that deposition was influenced by geostrophic currents in an epeiric sea with water depths of 500–800 m, where the sea floor had a considerable relief, commonly of more than a hundred metres amplitude, comprising moats, drifts, mounds and channels (Surlyk and Lykke-Andersen, 2007; Esmerode et al., 2008). The margins of the basin feature broad moat/trough-like channels that are juxtaposed next to accretionary forms of detrital carbonate and marl.

Thermohaline circulation in the deep ocean basins is driven by density differences between water masses due to variations in water temperature and salinity (see McCave et al., 1995 for a Quaternary example). Recently, the thermohaline circulation forms a large network of slowly moving currents flowing at a few centimetres per second, only periodically interrupted by higher current velocities and dominant erosion processes (Faugères and Mulder, 2011). Contour currents may carry in suspension muddy-silty fines and particulate organic matter, forming significant nepheloid (turbid) bottom water bodies (McCave, 1985, 2008; Rebesco et al., 2014). The Pliensbachian profile in Mochras is interpreted to represent such calcareous muddy and silty contourites, commonly interbedded with calcareous sandy contourites containing reworked shallow-water carbonate debris from off-shelf or off-ramp supply with variable admixture of siliciclastic material. The depositional rate at Mochras was stable and relatively high, probably due to biogenic input from shallower zones (carbonate platform), moderate or slow current velocity and weak erosion. Terrigenous (clays and fine silts) or carbonate (biogenic fragments) particles supplied by bottom currents may carry in suspension a considerable amount particulate organic matter, supplying food to deep-marine benthic organisms (Thistle et al., 1985). Likely, the deep-water circulation in the elongated, NE-SW trending Cardigan Basin (Fig. 2) was forced by enhanced geostrophic bottom-water circulation – i.e. cooler and denser waters flowing from the Boreal Sea, around the Shetland Platform-Scottish Landmass island, towards the south, to the Peri-Tethys/proto-Atlantic, approximately parallel to the bathymetric contours of the margin of the Welsh Platform (Figs. 1, 2).

Reconstructions of circulation that rely on numerical models (Bjerrum et al., 2001; Dera and Donnadieu, 2012; Ruvalcaba Baroni et al., 2018) have reached remarkably consistent conclusions about the predominant southwards flow from the Arctic into the Tethys through the Laurasian Seaway during Early Jurassic. The Cardigan Bay Strait, linking cooler and shallower waters of Boreal Sea and Scottish-English-Welsh archipelago with warmer and deeper waters of Peri-Tethys (Figs. 1, 2), was then situated to sustain a continuous thermohaline-driven geostrophic contour current circulation between these two marine realms. Thermohaline-driven geostrophic contour currents usually involve significant water mass over large areas and persist for very long time intervals of up to millions of years and over large areas (Shanmugam, 2008, 2017), which corresponds to the observed continuity of Early Jurassic sedimentation in Mochras. These stable flow conditions were punctuated by more sluggish currents or stagnant conditions.

Ruvalcaba Baroni et al. (2018) indicate that, under high atmospheric pCO_2, palaeoceanographic conditions in the Laurasian Seaway were dominated by strong clockwise circulation in the Tethys bringing warm saline waters onto European shelves. This strong circulation may have diminished the effects of flow through the Laurasian Seaway. Dera and Donnadieu (2012) concluded, that warming events, demise of polar sea ice, and stronger high-latitude continental runoff rates could result in a thermohaline circulation collapse and bottom oxygen depletion, also in deep oceanic settings. In contrast, lowered pCO_2 may have led to a decrease in the strength of Tethyan flow and enhanced the influence of Boreal influx (Korte et al., 2015; Van de Schootbrugge et al., 2019). Observed lithological and ichnological fluctuations are likely associated with intertwined periods of invigorated currents and more stagnant conditions, while nutrient availability seemed to be relatively stable and sufficient all the time (as shown by the TOC content; see Storm et al., 2020; Figs. 2, 3) and played a subordinate role in setting ichnological trends. Cyclic, hierarchical lithological and ichnological successions strongly point to a regular controlling mechanism, such as orbital forcing.

4.2. Ichnology and harmonic analysis

So far, there is no uniform model of bioturbation in contourites. Hitherto ichnological analysis of contourites has revealed changes in ichnofabric attributes over relatively short lateral distances, including trace fossil composition, cross-cutting relationships, or ichnofabric index (Hüneke and Stow, 2008; Wetzel et al., 2008; Wetzel and Uchman, 2012; Rodríguez-Tovar et al., 2016, 2017, 2019; Rodríguez-Tovar and Hernández-Molina, 2018; de Castro et al., 2020a, 2020b). Dorador et al. (2019) have indicated that the distance to the bottom current "core" exerts tangible influence on specific macro-benthic tracemaker communities in contourite deposits. This parameter itself reflects other bottom current features, such as hydrodynamic energy, grain size, nutrient transport, etc. Specifically, strong domination of *Phycosiphon* is unique for the Pliensbachian contourite deposits in Mochras. *Phycosiphon*, common in turbidites and hyperpycnites (e.g. Wetzel and Uchman, 2012; Knaust et al., 2014), is also reported from contourite deposits (Baldwin and McCave, 1999; Wetzel et al., 2008) but as a rare, subordinate trace fossil. Possibly, in previous papers diffuse *Phycosiphon* was simply described as “bioturbation”. In particular, this ichnotaxon could be difficult to recognize in recent, unconsolidated contourite deposits. As *Phycosiphon* is represented by four distinct morphotypes, Ph1–Ph4, they should be treated separately for further analysis of cyclicity. Ph2 is so frequent that it cannot be indicative for cyclic changes. However, three other morphotypes with more patchy appearance can be used. *Thalassinoides* and *Schaubcylindrichnus* are frequent enough to be used for analysis of cyclicity as well. Other ichnotaxa are not frequent enough for harmonic analysis, although their cyclic appearances yield important information concerning more general cycles hierarchy. In that context, it is noteworthy that *Zoophycos* has the potential of being used as a proxy for cyclical monsoon fluctuations at the Milankovitch scale covering the last 425 kyr from the northeastern South China Sea (Rodríguez-Tovar et al., 2011). Additionally, lamination can be used for such analysis (Supplementary 1).

The results of runs tests demonstrate the non-random nature of particular trace fossils and lamination distribution within the whole studied sedimentary succession (Supplementary 2). The absolute values of all resultant *Z*-scores are greater than critical value of 1.96, allowing rejection of the null hypothesis at the 95% confidence level.

The peak values of the Walsh power-spectra (Figs. 11, 12) match well the expected duration of the orbitally-forced periodicities (Table 1). Figs. 11 and 12 summarize the results of spectral analysis and present the correlation between them and the individual bands of orbital periodicities predicted by Berger (1977). The approach used to convert the results of spectral analysis to time values is explained in the “Material and methods” section. In addition to the main precession, obliquity and short eccentricity periodicities, their component and beat frequencies are reflected by the spectra (Tiwari, 1987; Negi et al., 1993). On the one hand, the shorter-term periodicities are expected to be recorded more precisely than the longer-term, as larger number of them is contained within the studied time series. On the other hand, they are potentially more prone to be blurred by inconstant sedimentation rate.

The interpreted precession and obliquity cycles are the most intensely represented on the spectrograms (Figs. 11, 12). The 18–23 kyr precession terms are clearly reflected by the sequency values of 0.85–1.15 cycles/m, corresponding to the visually determined 4th order cycles. Either one or more of the precessional bands are reflected by each of the analyzed time series. Despite not being readily distinguished visually in the sedimentary succession, the main obliquity term is distinctly present in the spectra of all analyzed time series. Furthermore, the periodicity of circa 29 kyr is observed in the occurrences of *Phycosiphon* (Ph4) (Fig. 11C) and lamination (Fig. 12C), which probably lies in the shortest obliquity term (Tiwari, 1987; Laskar et al., 2011). The longest obliquity term is presumably recorded by 54.6 kyr periodicity of *Phycosiphon* morphotypes Ph1 and Ph3 (Fig. 12A). The spectrogram based on the *Thalassinoides* occurrences (Fig. 11D) displays the peak near 0.34 cycles/m value, which can be associated with the combined effect of obliquity and precession as proposed by Berger (1977).

The 94.4 kyr periodicity recorded by *Schaubcylindrichnus* and lamination (Fig. 12C) and ~100 kyr periodicity recorded by *Phycosiphon* type Ph1 (Figs. 11A, 12A) can be identified as the shortest term of short eccentricity cycles, presumably reflecting the 3rd order cycles distinguished in the sedimentary and ichnological record (Figs. 3, 4). The longer term of short eccentricity is interpreted to be displayed by the *Phycosiphon* type Ph4 (often related to *Thalassinoides*) periodicity of 115.4 kyr term (Figs. 11C, 12B). *Phycosiphon* types Ph1 and Ph4 record also the periodicity of c. 166 kyr term which likely can reflect a cycle of non-orbital origin. The peak clusters present in the leftmost parts of the spectrograms may presumably be associated with 2nd order cycles (registered by recurrent appearances of cf. *Polykladichnus* and other dwelling structures, which were not included in the harmonic analysis due to their low frequency). However, low resolution of the spectra below the sequency values of 0.1 cycles/m hinders the calibration of these peaks to the time domain. In particular, *Schaubcylindrichnus* and lamination (Fig. 12C) clearly display the frequencies of the shortest eccentricity term (c. 95 kyr), the shortest obliquity term (c. 29–30 kyr) and the longest precessional term (c. 21–22 kyr).

Counted numbers of precession (4th order) cycles, compared with inferred durations of successive ammonite zones (Table 3) show that average durations of these cycles within each zone slightly fluctuated (although generally stayed within relatively stable 21.7–25.8 kyr precessional term – 23.62 in average). Duration of an average 4th order cycle decreased gradually from 24.8 kyr (*jamesoni* Zone), through 23.5 kyr (*ibex* Zone) to minimum 21.7 kyr (*davoei* Zone), and then increased to 22.3 kyr (*margaritatus* Zone) and back to longer 25.8 kyr duration (*spinatum* Zone). This can be explained by eccentricity modulation of climatic precession (cf. Huybers and Aharonson, 2010). Although the influence of eccentricity on the amplitude of precession forcing is more widely appreciated than its influence upon the frequency, there also exists a relationship between eccentricity and the frequency of precession. The frequency of climatic precession undergoes variations particularly when the eccentricity of Earth's orbit is small (Huybers and Aharonson, 2010). Interestingly, the whole “wandering frequency” cycle would span (possibly together with the earliest *tenuicostatum* Zone of Toarcian) c. 9 Myr. On the other hand, the changing average duration might be due to missing cycles where the durations seem over-long.

Longer-term “grand cycles” which are not included in harmonic analysis are characterized by gradually growing and subsequently falling ichnodiversity and $CaCO_3$ separated by clayey, $CaCO_3$ poor, often laminated intervals devoid of trace fossils, marking "grand cycle" boundaries (Figs. 1, 2). Judging from duration of ~100 kyr and ~400 kyr eccentricity cycles, these longer-term eccentricity “grand cycles”

Table 3
Duration and sedimentation rate of Pliensbachian biochronozones - comparison of results obtained by Ruhl et al. (2016), Storm et al. (2020) and by present authors. Note much shorter duration obtained herein for the *spinatum* Zone, otherwise the results are approximately consistent.

Stage	Ammonite Zone	Thickness (m)	Relative duration elemental Ca (Ruhl et al., 2016) **(Myr)**	Relative duration $\delta^{13}C_{TOC}$ (Storm et al., 2020) **(Myr)**	Relative duration ichnology (this paper) **(Myr)**	Sedimen-tation rate (Ruhl et al., 2016) **-cm/1000 years**	Sedimen-tation rate (Storm et al., 2020) **- cm/1000 years**	Sedimen-tation rate (this paper) **-cm/1000 years**
Pliensbachian – **387 m**	*spinatum*	**37**	1.4 (**Σ 8.7**)	1.45 (**Σ 8.77**)	0.8 (**Σ 8.4**)	2.6 cm/1kyr	2.6 cm/1kyr	4.6 cm/1kyr
	margaritatus	**110**	2.4	2.69	2.33	4.6 cm/1kyr	4.1 cm/1kyr	4.7 cm/1kyr
	davoei	**24**	0.4	0.45	0.47	6 cm/1kyr	5.3 cm/1kyr	5,1 cm/1kyr
	ibex	**90**	1.8	1.76	2.0	5 cm/1kyr	5.1 cm/1kyr	4.5 cm/1kyr
	jamesoni	**126**	2.7	2.43	2.8	4.7 cm/1kyr	5.2 cm/1kyr	4.5 cm/1kyr

would be of duration c. 2.5 Myr, corresponding to the period of around 2.4 Myr eccentricity modulation related with Mesozoic greenhouse sequences, caused by Earth-Mars secular resonance (Hinnov, 2000; Laskar et al., 2004, 2011). These ~2.5 Myr cycles are characterized by long-term shifts in $CaCO_3$ content and ichnodiversity, correlated with the variations in the opposing proportions of smectite and kaolinite. The kaolinite-rich intervals reflect an intensification of hydrolysis and an acceleration of the hydrological cycle, while the smectite-rich intervals indicate a more seasonally arid climate (Deconinck et al., 2019). In turn, kaolinite-rich intervals were connected with high atmospheric pCO_2, higher temperatures and influx of Tethyan warm saline waters onto European shelves (Ruvalcaba Baroni et al., 2018), diminishing flow through the Cardigan Bay Strait, which caused oxygen deficiency and reduced ichnodiversity at the "grand cycle" boundaries. On the other hand, lower pCO_2 and cooler conditions favoured intensification of currents, higher oxygenation and higher ichnodiversity, additionally enhanced by limited domination of *Phycosiphon*, mainly caused by presence of smectite. It would indicate that changes of ichnodiversity was mainly controlled by orbitally-forced current intensity, where most general changes were associated with “grand eccentricity cycles” of ~2.5 Myr duration.

Diminished current flow/oxygen depletion in the Cardigan Bay Strait appears particularly severe at the very end of Pliensbachian (continuing to the beginning of Toarcian *tenuicostatum* Zone), but also the beginning of Pliensbachian is characterized by relatively more marked oxygen depletion and *Phycosiphon* crisis, compared to the other (c. 2.5 Myr) “grand eccentricity cycles” boundaries in Pliensbachian. The mentioned above “wandering frequency” fluctuation would span ~9 Myr. As we have only one such sequence, it is not clear, if this represents a real cycle. However, existence of c. 9 Myr eccentricity cycle was postulated by Martinez and Dera (2015), based on analysis of orbital pacing of carbon cycle during the Mesozoic (spanning c. 70 Myr of Jurassic and Cretaceous periods). According to those authors, this orbital forcing affected carbon transfers by modulating the hydrological processes and sea-level changes, being an important metronome of the greenhouse climate dynamics. However, this question remains open until a longer time interval in Mochras and Prees is studied, particularly as Martinez and Dera (2015) did not see such a cycle specifically in Pliensbachian, attributed to major palaeoenvironmental disturbances or a chaotic transition affecting this cycle.

4.3. Duration of the Pliensbachian and the ammonite biozones based on ichnological astrochronology

The new results (Table 2) allow a re-estimation of the duration of Pliensbachian stage at about 8.4 Myr, which is shorter by ~0.3–0.4 Myr compared to the results obtained from elemental Ca content (8.7 Myr – Ruhl et al., 2016) and $\delta^{13}C_{TOC}$ (8.77 Mya – Storm et al., 2020). Results obtained from ichnological and sedimentological signals by counting successive 4th, 3rd and 2nd order cycles (interpreted respectively as precession/obliquity, short eccentricity, long eccentricity) (Figs. 3, 4, 11, 12; Tables 1–3) also show much more stable sedimentation rate in successive ammonite zones than the results based on elemental Ca or $\delta^{13}C_{TOC}$. Astronomical durations for the ammonite biozones are: *jamesoni* Zone = 2.8 Myr, *ibex* Zone = 2.0 Myr, *davoei* Zone = 0.47 Myr, *margaritatus* Zone = 2.33 Myr and *spinatum* Zone = 0.8 Myr. The *jamesoni* Zone is slightly longer (by ~100 kyr) than determined by Ruhl et al. (2016) and more significantly longer than the value of ~2.43 Myr obtained by Storm et al. (2020). The *ibex* Zone (2.0 Myr) and *davoei* Zone (0.47 Myr) would be slightly longer than 1.8 Myr and 0.45 Myr, respectively (by Ruhl et al., 2016) or 1.76 Myr and 0.4 Myr (by Storm et al., 2020). On the other hand, duration of the *margaritatus* Zone based on ichnological cycles (2.33 Myr) is shorter in comparison to 2.4 Myr (Ruhl et al., 2016) or 2.69 Myr (Storm et al., 2020). The most significant difference regards the *spinatum* Zone, which is much shorter than the values provided by Ruhl et al. (2016) and Storm et al. (2020), i.e. 1.4 and 1.45 Myr, respectively. Consequently, results obtained by Ruhl et al. (2016) and Storm et al. (2020) imply radically slower sedimentation rate (~2.6 cm/kyr) for the *spinatum* Zone in comparison to the older biozones (4.1–6.0 cm/kyr). This difference cannot be explained by conspicuous changes in the sedimentary environment; only the uppermost few metres of the *spinatum* Zone section shows marked changes in lithology and ichnology, associated with carbonate crisis and oxygen depletion and possible changes in sedimentary rate. As shown by Storm et al. (2020), the $\delta^{13}C_{TOC}$ signals in this zone are not unequivocal when we adopt an option of two long-eccentricity cycles in the *spinatum* Zone (Storm et al., 2020; Fig. 4, Table 1), calculation of the *spinatum* Zone duration and total duration of Pliensbachian would be approximately consistent with results obtained from ichnological signal. Radioisotopic dates from the upper Pliensbachian in Oregon, United States (De Lena et al., 2019), are correlated to the *margaritatus* and *spinatum* zones using good ammonite-based constraints, albeit primarily for the North American zonal scheme. These dates range from 186.96 +/− 0.07 Ma in the *kunae* Zone (i.e. lower *margaritatus* Zone) to 184.02 +/− 0.05 Ma, which lies above the highest ammonites of the *carlottense* Zone (i.e., approximately upper *spinatum* Zone or lower Toarcian *tenuicostatum* Zone). About 3 Myr duration of *margaritatus* and *spinatum* zones combined (with approximately a 2 Myr long *margaritatus* Zone and a 1 Myr long *spinatum* Zone) corresponds to our estimates of duration of these two zones (Table 2). The ichnological cycles are quite consistent with those interpreted by Ruhl et al. (2016) and Storm et al. (2020) for the *jamesoni*, *ibex* and *davoei* zones, with offsets usually less than 100 kyr (one short-eccentricity cycle). More discrepancies with cycles based on Ca appear in *margaritatus* Zone and we suggest this results from common $CaCO_3$ cementation producing numerous diffuse concretions observed in this zone. Rapid decrease of $CaCO_3$ content in the *spinatum* Zone also negatively affects the reliability of the Ca elemental signal for cycle analysis. The ichnological signal (supported by high-resolution lithological, sedimentological and clay mineral data) may thus be the most reliable source of the orbital forcing signal, providing also a better fit to the ~2.5 Myr 1st order "grand" cycles.

5. Conclusions

1. An integrated ichnological-sedimentological study of the Pliensbachian calcareous-siliciclastic hemipelagic/contourite deposits in

Mochras helps facilitate understanding of contourite deposition processes in a long period of geological time and its ichnodiversity. The current study adds the most expanded ichnological and sedimentary record of contourite deposits, giving new information on the sedimentary dynamics, variability of oceanographic history, and basin interconnectivity.
2. *Phycosiphon* is by far the most common ichnotaxon and this is a new observation, because in the literature to date this taxon was considered sporadic in contourite deposits. Ichnological signals point to a common and strongly repetitive mechanism driving the observed fluctuations in benthic conditions, which is indicated by harmonic analysis and distinction of four hierarchical orders of cycles attributed to orbital forcing.
3. Long-term climate changes had consequences for deep-sea sediments at Mochras as increased content of expandable clay minerals (smectite and mixed-layer clay minerals) reduced pore space, thus limiting development of *Phycosiphon* tracemakers and allowing other organisms which were less dependent on pore-space oxygen, to compete with otherwise dominating *Phycosiphon* trace makers.
4. The ichnological record shows a relatively stable sedimentation rate of 4.5–5.1 cm/kyr through the entire Pliensbachian stage.
5. Ichnological results (both macroscopic observations and harmonic analysis) support that the cycles that appear in the Mochras logs, previously indicated by Ruhl et al. (2016) and Storm et al. (2020) are astronomically forced, although their frequency through individual zones are refined and a new calibration of duration of Pliensbachian (c. 8.4 Myr) and successive ammonite zones is proposed.
6. Orbital forcing has set the timing for cyclic ichnological records, with the amplifying feedback of climate-related palaeoceanographic variations of thermohaline-driven geostrophic contour currents circulating between Boreal ocean and Peri-Tethys, through the Cardigan Bay Strait.
7. Contourites of the Cardigan Bay Basin provide essential information on ocean circulation, bottom life conditions and climate changes, which can be extracted using sedimentological and ichnological methods. The Cardigan Bay Strait played an important role in the Early Jurassic (at least Pliensbachian) oceanic circulation as a major link between the northern and southern part of the Laurasian Seaway, and in general between the Boreal and Peri-Tethys domains.
8. Ichnological records in continuous hemipelagic successions seem to be a sensitive and reliable basis for recognition of orbital forcing of cyclic climatic and palaeoceanographic changes.

Declaration of Competing Interest

The authors declare that they have no known competing financial interests or personal relationships that could have appeared to influence the work reported in this paper.

Acknowledgements

The research is financed by the National Science Centre, Poland, from the programme Opus 13, grant agreement No2017/25/B/ST10/02235 and the Internal Polish Geological Institute grant no. 62.9012.2016.00.0. We thank the editor, Maoyan Zhu and two anonymous Reviewers for their comments, which helped us to improve the manuscript. This is a contribution to the ICDP and NERC project JET (grant number NE/N018508/1).

Appendix A. Supplementary data

Supplementary data to this article can be found online at https://doi.org/10.1016/j.gloplacha.2021.103648.

References

Alpert, S.P., 1974. Systematic review of the genus *Skolithos*. J. Paleont. 49, 509–521.
Archer, D., Emerson, S., Reimers, C., 1989. Dissolution of calcite in deep-sea sediments: pH and O_2 microelectrode results. Geochim. Cosmochim. Acta 53, 2831–2845.
Ausich, W.I., Bottjer, D.J., 1982. Tiering in suspension-feeding communities on soft substrata throughout the Phanerozoic. Science 216, 173–174.
Ayranci, K., Harris, N.B., Dong, T., 2018. High resolution sequence stratigraphic reconstruction of mud-dominated systems below storm wave base; a case study from the Middle to Upper Devonian Horn River Group, British Columbia, Canada. Sediment. Geol. 373, 239–253.
Baldwin, C.T., McCave, I.N., 1999. Bioturbation in an active deep-sea area: implications for models of trace fossil tiering. Palaios 14, 375–388.
Barth, G., Pieńkowski, G., Zimmermann, J., Franz, M., Kuhlmann, G., 2018. Palaeogeographical evolution of the Lower Jurassic: high-resolution biostratigraphy and sequence stratigraphy in the Central European Basin. In: Kilhams, B., Kukla, P. A., Mazur, S., McKie, T., Mijnlieff, H.F., Van Ojik, K. (Eds.), Mesozoic Resource Potential in the Southern Permian Basin. Geological Soc., London, Spec. Publ, 469, pp. 341–369. https://doi.org/10.1144/SP469.8.
Bednarz, M., McIlroy, D., 2009. Three-dimensional reconstruction of "phycosiphoniform" burrows: implications for identification of trace fossils in core. Palaeontol. Electron. 12 (3), 13A (15 pp).
Bein, A., Weiler, Y., 1976. The cretaceous Talme Yafe Formation: a contour current shaped sedimentary prism of calcareous detritus at the continental margin of the Arabian craton. Sedimentology 23, 511–532.
Berger, A.L., 1977. Support for the astronomical theory of climatic change. Nature 269, 44–45.
Bjerrum, C.J., Surlyk, F., Callomon, J.H., Slingerland, R.L., 2001. Numerical paleoceanographic study of the early Jurassic Transcontinental Laurasian seaway. Paleoceanography 16, 390–404.
Borisov, D.G., Murdmaa, I.O., Ivanova, E.V., Levchenko, O.V., Yutsis, V.V., Frantseva, T. N., 2013. Contourite systems in the region of the Southern São Paulo Plateau escarpment, South Atlantic. Oceanology 53, 460–471.
Boulila, S., Galbrun, B., Miller, K.G., Pekar, S.F., Browning, J.V., Laskar, J., Wrigh, James D., 2011. On the origin of Cenozoic and Mesozoic "third-order" eustatic sequences. Earth Sci. Rev. 109, 94–112.
Bouma, A.H., 1962. Sedimentology of some Flysch Deposits. Elsevier, Amsterdam (168 pp).
Bromley, R.G., 1991. *Zoophycos*: strip mine, refuse dump, cache or sewage farm? Lethaia 24, 460–462.
Bromley, R.G., 1996. Trace fossils. In: Biology, Taphonomy and Applications, Second ed. Chapman & Hall, London. (361 pp).
Bromley, R.G., Ekdale, A.A., 1986. Composite ichnofabric and tiering burrows. Geol. Mag. 123, 49–65.
Bromley, R.G., Uchman, A., 2003. Trace fossils from the lower and Middle Jurassic marginal marine deposits of the Sorthat Formation, Bornholm, Denmark. Bull. Geol. Soc. Denm. 52, 185–208.
Callow, R.H.T., McIlroy, D., Kneller, B., Dykstra, M., 2013. Integrated ichnological and sedimentological analysis of a late cretaceous submarine channel-levee system: the Rosario Formation, Baja California, Mexico. Mar. Pet. Geol. 41, 277–294.
Caswell, B.A., Frid, C.L.J., 2017. Marine ecosystem resilience during extreme deoxygenation: the early Jurassic oceanic anoxic event. Oecologia 183, 275–290. https://doi.org/10.1007/s00442-016-3747-6.
Cope, J.C.W., Ingham, J.K., Rawson, P.F. (Eds.), 1992. Atlas of Palaeogeography and Lithofacies. Geological Society, London, Memoir, 13.
Copestake, P., Johnson, B., 2014. Lower Jurassic Foraminifera from the Llanbedr (Mochras Farm) Borehole, North/Wales, UK, 167. Monograph of the Palaeontographical Society, London, pp. 1–403.
Crimes, T.P., 1977. Trace fossils of an Eocene deep-sea fan, northern Spain. In: Crimes, T. P., Harper, J.C. (Eds.), Trace Fossils 2, Geol. Jour. Spec. Issue, vol. 9, pp. 71–90.
Dashtgard, S.E., 2011. Neoichnology of the lower delta plain: Fraser River Delta, British Columbia, Canada: Implications for the ichnology of deltas. Palaeogeogr. Palaeoclimatol. Palaeoecol. 307, 98–108.
de Castro, S., Hernández-Molina, F.J., Rodríguez-Tovar, F.J., Llave, E., Ng, Z.L., Nishida, N., Mena, A., 2020a. Contourites and bottom current reworked sands: Bed facies model and implications. Mar. Geol. 428, 106267.
de Castro, S., Hernández-Molina, F.J., De Weger, W., Jimenez-Espejo, F.J., Rodríguez-Tovar, F.J., Mena, A., Llave, E., Sierro, F.J., 2020b. Contourite characterization and its discrimination from other deep-water deposits in the Gulf of Cadiz contourite depositional system. Sedimentology 68. https://doi.org/10.1111/sed.12813.
de Graciansky, P.C., Jacquin, T., Hesselbo, P.S., 1998. The Ligurian cycle: an overview of lower Jurassic 2nd-order transgressive/regressive facies cycles in Western Europe. In: de Graciansky, P.C., Hardenbol, J., Jacquin, T., Vail, P.R. (Eds.), Mesozoic and Cenozoic Sequence Stratigraphy of European Basins, 60. Soc. Econ. Paleont. Miner. Spec. Publ., pp. 467–479
De Lena, L.F., Taylor, D., Guex, J., Bartolini, A., Adatte, T., van Acken, D., Spangenberg, J.E., Samankassou, E., Vennemann, T., Schaltegger, U., 2019. The driving mechanisms of the carbon cycle perturbations in the late Pliensbachian (early Jurassic). Sci. Rep. 9, 18430.
Deconinck, J.F., Hesselbo, S.P., Pellenard, P., 2019. Climatic and sea-level control of Jurassic (Pliensbachian) clay mineral sedimentation in the Cardigan Bay Basin, Llanbedr (Mochras Farm) borehole Wales. Sedimentology 66, 2769–2783.
Dera, G., Donnadieu, Y., 2012. Modeling evidences for global warming, Arctic seawater freshening, and sluggish oceanic circulation during the early Toarcian anoxic event. Paleoceanography 27, PA2211. https://doi.org/10.1029/2012PA002283.

Dera, G., Neige, P., Dommergues, J.-L., Brayard, A., 2011. Ammonite paleobiogeography during the Pliensbachian–Toarcian crisis (early Jurassic) reflecting paleoclimate, eustasy, and extinctions. Glob. Planet. Chang. 78, 92–105.

Dobson, M.R., Whittington, R.J., 1987. The geology of Cardigan Bay. Proc. Geol. Assoc. 98, 331–353.

Dorador, J., Rodríguez-Tovar, F.J., Mena, A., Francés, G., 2019. Lateral variability of ichnological content in muddy contourites: Weak bottom currents affecting organisms' behavior. Sci. Rep. 9, 17713. https://doi.org/10.1038/s41598-019-54246-3.

Dunham, R.J., 1962. Classification of carbonate Rocks according to depositional texture. In: Ham, W.E. (Ed.), Classification of Carbonate Rocks, AAPG Memoir, vol. 1, pp. 108–121.

Ehrenberg, K., 1944. Ergänzende Bemerkungen zu den seinerzeit aus dem Miozäan von Burgschleinitz beschrieben Gangkernen und Bauten dekapoder Krebse. Paläont. Zeitschr. 23, 354–359.

Ekdale, A.A., 1992. Muckraking and mudslinging: The joys of deposit-feeding. In: Maples, C.G., West, R.R. (Eds.), Trace Fossils, Short Cours. Paleont, vol. 5. The Paleontological Society, Knoxville, Tennessee, pp. 145–171.

Ekdale, A.A., Lewis, D.W., 1991. The New Zealand *Zoophycos* revisited. Ichnos 1, 183–194.

Erba, E., Premoli Silva, I., 1994. Orbitally driven cycles in trace-fossil distribution from the Piobicco core (late Albian, Central Italy). Spec. Publ. Inst. Ass. Sediment. 19, 211–225.

Esmerode, E.V., Lykke-Andersen, H., Surlyk, F., 2008. Interaction between bottom currents and slope failure in the late cretaceous of the southern Danish Central Graben, North Sea. J. Geol. Soc. Lond. 165, 55–72.

Etienne, S., Mulder, T., Razin, P., Bez, M., Tournadour, E., 2014. Proximal to distal turbiditic sheet-sand heterogeneities: Characteristics of associated internal channels. Examples from the Trois Evêchés area, Eocene-Oligocene Annot Sandstones (Grès d'Annot), SE France. Mar. Pet. Geol. 41, 117–133.

Ewing, M., Thorndike, E.M., 1965. Suspended matter in deep ocean waters. Science 147, 1291–1294.

Farrow, G.E., 1966. Bathymetric zonation of Jurassic trace fossils from the coast Yorkshire, England. Palaeogeogr. Palaeoclimatol. Palaeoecol. 2, 103–151.

Faugères, J.C., Mulder, T., 2011. Contour currents and contourite drifts. In: Huneke, H., Mulder, T. (Eds.), Deep-Sea Sediments, Developments in Sedimentology, vol. 63. Elsevier, Amsterdam, pp. 149–214.

Faugères, J.-C., Stow, D.A.V., 2008. Contourite drifts: nature, evolution and controls. In: Rebesco, M., Camerlenghi, A. (Eds.), Contourites, Developments in Sedimentology, vol. 60. Elsevier, Amsterdam, pp. 257–288.

Faugères, J.-C., Gonthier, E., Stow, D.A.V., 1984. Contourite drift moulded by deep Mediterranean outflow. Geology 12, 296–300.

Fillion, D., Pickerill, R.K., 1990. Ichnology of the upper Cambrian? To lower Ordovician Bell Island and Wabana groups of eastern Newfoundland, Canada. Palaeontogr. Can. 7, 1–119.

Fischer-Ooster, C., 1858. Die fossilen Fucoiden der Schweizer-Alpen, nebst Erörterungen über deren geologisches Alter. Huber, Bern (72 pp).

Frey, R.W., 1970. Trace fossils of Fort Hays Limestone Member of Niobrara Chalk (Upper cretaceous) West-Central Kansas. Univ. Kansas Paleont. Contrib. 53, 1–41.

Frey, R.W., Bromley, R.G., 1985. Ichnology of American chalks: the Seelma Group (Upper cretaceous), western Alabama. Can. J. Earth Sci. 22, 801–822.

Frey, R.W., Goldring, R., 1992. Marine event beds and recolonization surfaces as revealed by trace fossil analysis. Geol. Mag. 129, 325–335.

Frey, R.W., Howard, J.D., 1981. *Conichnus* and *Schaubcylindrichnus*: redefined trace fossils from the Upper cretaceous of the Western Interior. J. Paleont. 55, 800–804.

Frey, R.W., Howard, J.D., Pryor, W.A., 1978. *Ophiomorpha*: its morphologic, taxonomic, and environmental significance. Palaeogeogr. Palaeoclimatol. Palaeoecol. 23, 199–223.

Frey, R.W., Curran, A.H., Pemberton, G.S., 1984. Trace making activities of crabs and their environmental significance: the ichnogenus *Psilonichnus*. J. Paleont. 58, 333–350.

Fu, S., 1991. Funktion, Verhalten und Einteilung fucoider und lophocteniider Lebensspuren. Courier Forsch. Senckenberg 135, 1–79.

Fürsich, F.T., 1973. A revision of the trace fossils *Spongeliomorpha*, *Ophiomorpha* and *Thalassinoides*. N. Jb. Geol. Pal. Mh. 1973 (12), 719–735.

Fürsich, F.T., 1974. Ichnogenus *Rhizocorallium*. Paläont. Zeitschr. 48, 16–28.

Fürsich, F.T., 1981. Invertebrate trace fossils from the Upper Jurassic of Portugal. Comun. Serv. Geol. Portugal 67, 153–168.

Fürsich, F.T., Mayr, H., 1981. Non-marine *Rhizocorallium* (trace fossil) from the Upper Freshwater Molasse (Upper Miocene) of southern Germany. N. Jb. Geol. Paläont. Mh. 1981 (6), 321–333.

Gingras, M.K., Dashtgard, S.E., MacEachern, J.A., Pemberton, S.G., 2008. Biology of shallow-marine ichnology: a modern perspective. Aquat. Biol. 2, 255–268.

Goldring, R., 1962. Trace fossils of the Baggy Beds (Upper Devonian) of North Devon, England. Paläont. Zeitschr. 36, 232–251.

Goldring, R., Pollard, J.E., Taylor, A.M., 1991. *Anconichnus horizontalis*: a pervasive ichnofabric-forming trace fossil in the post-Paleozoic offshore siliciclastic facies. Palaios 6, 250–263.

Gong, C., Peakall, J., Wang, Y., Wells, M.G., Xu, J., 2017. Flow processes and sedimentation in contourite channels on the northwestern South China Sea margin: a joint 3D seismic and oceanographic perspective. Mar. Geol. 393, 176–193.

Gross, T.F., Williams, A.J., 1991. Characterisation of deep-sea storms. Mar. Geol. 99, 281–301.

Hakes, W.G., 1976. Trace fossils and depositional environment of four clastic units, Upper Pennsylvanian megacyclothems, Northeast Kansas. Univ. Kansas Palaeont. Contrib. 63, 1–46.

Haldeman, S.S., 1840. Suplement to Number One of "a Monograph of the Limniades, and Other Freshwater Univalve Shells of North America", Containing Descriptions of Apparently New Animals in Different Classes, and Names and Characters of the Subgenera in *Paludina* and *Anculosa*. J. Dobson, Philadelfia (3 pp).

Hall, J., 1847. Paleontology of New York, vol. 1. C. Van Benthuysen, Albany (338 pp).

Hallam, A., Swett, K., 1966. Trace fossils from the lower Cambrian Pipe Rock of the north-west Highlands. Scott. J. Geol. 2, 101–106.

Hammer, Ø., Harper, D.A.T., 2006. Paleontological Data Analysis. Blackwell, Oxford.

Hammer, Ø., Harper, D.A.T., Ryan, P.D., 2001. PAST: Paleontological statistics software package for education and data analysis. Palaeontol. Electron. 4 (1) (9 pp).

Hesselbo, S.P., 2008. Sequence stratigraphy and inferred relative sea-level change from the onshore British Jurassic. Proc. Geol. Assoc. 119, 19–34.

Hesselbo, S.P., Jenkyns, H.C., 1995. A comparison of the Hettangian to Bajocian successions of Dorset and Yorkshire. In: Taylor, P.D. (Ed.), Field Geology of the British Jurassic. Geological Society, London, pp. 105–150.

Hesselbo, S.P., Bjerrum, C.J., Hinnov, L.A., MacNiocaill, C., Miller, K.G., Riding, J.B., Van de Schootbrugge, B., the Mochras Revisited Science Team, 2013. Mochras borehole revisited: a new global standard for early Jurassic Earth history. Sci. Drill. 16, 81–91. https://doi.org/10.5194/sd-16-81-2013.

Hinnov, L.A., 2000. New perspectives on orbitally forced stratigraphy. Annu. Rev. Earth Planet. Sci. 28, 419–475.

Hüneke, N.V., Stow, D.A.V., 2008. Identification of ancient contourites: Problems and palaeoceanographic significance. In: Rebesco, M., Camerlenghi, A. (Eds.), Contourites, Developments in Sedimentology, vol. 60, pp. 323–344.

Huybers, P., Aharonson, O., 2010. Orbital tuning, eccentricity, and the frequency modulation of climatic precession. Paleoceanography 25, PA4228. https://doi.org/10.1029/2010PA00195225(4).

Izumi, K., 2012. Formation process of the trace fossil *Phymatoderma granulata* in the lower Jurassic black shale (Posidonia Shale, southern Germany) and its paleoecological implications. Palaeogeogr. Palaeoclimatol. Palaeoecol. 353–355, 116–122.

Izumi, K., 2014. Utility of geochemical analysis of trace fossils: case studies using Phycosiphon incertum from the lower Jurassic shallow-marine (Higashinagano Formation, Southwest Japan) and Pliocene deep-marine deposits (Shiramazu Formation, Central Japan). Ichnos 21, 62–72.

Jensen, S., 1997. Trace fossils from the lower Cambrian Mickwitzia Sandstone, south-Central Sweden. Fossils Strata 42, 1–110.

Kędzierski, M., Uchman, A., Sawłowicz, Z., Briguglio, A., 2015. Fossilized bioelectric wire – the trace fossil *Trichichnus*. Biogeosciences 12, 2301–2309.

Kennedy, W.J., 1975. Trace fossils in carbonate rocks. In: Frey, R.W. (Ed.), The Study of Trace Fossils. Springer-Verlag, New York, pp. 377–398.

Kjeldsen, K.U., Schreiber, L., Thorup, C.A., Boesen, T., Bjerg, J.T., Yang, T., Dueholm, M. S., Larsen, S., Risgaard-Petersen, N., Nierychlo, M., Schmid, M., Bøggild, A., van de Vossenberg, J., Geelhoedi, J.S., Meysman, F.J.R., Wagner, M., Nielsen, P.H., Nielsena, L.P., Schramm, A., 2019. On the evolution and physiology of cable bacteria. Proc. Natl. Acad. Sci. U. S. A. 116, 19116–19125.

Knapp, L.J., McMillan, J.M., Harris, N.B., 2017. A depositional model for organic-rich Duvernay Formation mudstones. Sediment. Geol. 347, 160–182.

Knaust, D., 2013. The ichnogenus *Rhizocorallium*: Classification, trace makers, palaeoenvironments and evolution. Earth-Sci. Rev. 126, 1–47.

Knaust, D., 2015. Siphonichnidae (new ichnofamily) attributed to the burrowing activity of bivalves: Ichnotaxonomy, behaviour and palaeoenvironmental implications. Earth-Sci. Rev. 150, 497–519.

Knaust, D., 2017. Atlas of Trace Fossils in Well Core: Appearance, Taxonomy and Interpretation. Springer (271 pp).

Knaust, D., Warchoł, M., Kane, I.A., 2014. Ichnodiversity and ichnoabundance: Revealing depositional trends in a confined turbidite system. Sedimentology 61, 2218–2267.

Korte, C., Hesselbo, S.P., Ullmann, C.V., Dietl, G., Ruhl, M., Schweigert, G., Thibault, T., 2015. Jurassic climate mode governed by ocean gateway. Nat. Commun. 6, 10015.

Kotake, N., 1992. Deep-sea echiurans: possible producers of *Zoophycos*. Lethaia 25, 311–316.

Kotlarczyk, J., Uchman, A., 2012. Integrated ichnology and ichthyology of the Oligocene Menilite Formation, Skole and Subsilesian nappes, Polish Carpathians: a proxy to oxygenation history. Palaeogeogr. Palaeoclimatol. Palaeoecol. 331–332, 104–118.

Krobicki, M., Tyszka, J., Uchman, A., Bąk, M., 2006. Stop A2 – Flaki Range (Fig. A12B) – Branisko Succesion (Bajocian–Oxfordian). In: Wierzbowski, A., Aubrecht, R., Golonka, J., Gutowski, J., Krobicki, M., Matyja, B.A., Pieńkowski, G., Uchman, A. (Eds.), Jurassic of Poland and Adjacent Slovakian Carpathians, Filed Trip Guidebook of 7th International Congress on the Jurassic System, Poland, Kraków, September, 6–18, 2006. Polish Geological Institute, Warsaw, pp. 29–34.

Laskar, J., Robutel, P., Joutel, F., Gastineau, M., Correia, A.C.M., Levrard, B., 2004. A longterm numerical solution for the insolation quantities of the Earth. Astron. Astrophys. 428, 261–285.

Laskar, J., Fienga, A., Gastineau, M., Manche, H., 2011. La2010: a new orbital solution for the long term motion of the Earth. Astron. Astrophys. 532, A89. https://doi.org/10.1051/0004-6361/201116836.

Locklair, R.E., Savrda, C.E., 1998. Ichnology of rhythmically bedded Demopolis Chalk (Upper cretaceous, Alabama): Implications for paleoenvironment, depositional cycle origins, and tracemaker behavior. Palaios 13, 423–438.

Lord, N.S., Ridgwell, A., Thorne, M.C., Lunt, D.J., 2016. An impulse response function for the "long tail" of excess atmospheric CO_2 in an Earth system model. Global Biogeochem. Cycl. 30, 2–17. https://doi.org/10.1002/2014GB005074.

Löwemark, L., Nara, M., 2013. Morphological variability of the trace fossil *Schaubcylindrichnus coronus* as a response to environmental forcing. Palaeontol. Electron. 16, 5A (14 pp).

Löwemark, L., Lin, I., Sarnthein, M., 2006. Temporal variations of the trace fossil *Zoophycos* in a 425 k.y.-long sediment record from the South China Sea: implications for the ethology of the *Zoophycos*-producer. Geol. Mag. 143, 105–114.
MacEachern, J.A., Burton, J.A., 2000. Firmground *Zoophycos* in the lower cretaceous Viking formation, Alberta: a distal expression of the *Glossifungites* ichnofacies. Palaios 15, 387–398.
Maiti, S., Tiwari, R.K., 2012. Modeling of rock boundary using Walsh Domain Sequency Filtering: An example from the German Continental Deep Drilling Program (KTB) Borehole Site. In: 9th Biennial International Conference & Exposition on Petroleum Geophysics. Society of Petroleum Geophysicists (SPG), Hyderabad 2012, P-019 (7 pp).
Mángano, M.G., Buatois, L.A., 1991. Discontinuity surfaces in the lower Cretaceus of the High Andes (Mendoza, Argentina): trace fossils and environmental implications. J. S. Am. Earth Sci. 4, 215–299.
Martinez, M., Dera, G., 2015. Orbital pacing of carbon fluxes by a ~9-my eccentricity cycle during the Mesozoic. Proc. Natl. Acad. Sci. 112, 12604–12609.
Martos, Y., Maldonado, A., Lobo, F.J., Hernández-Molina, F.J., Pérez, L.F., 2013. Tectonics and palaeoceanographic evolution recorded by contourite features in southern Drake Passage (Antarctica). Mar. Geol. 343, 73–91.
Massalongo, A., 1855. *Zoophycos*, Novum Genus Plantorum Fossilium. Verona, Antonelli (52 pp).
Mayer, L.M., 1994. Surface area control of organic carbon accumulation in continental shelf sediments. Geochim. Cosmochim. Acta 58, 1271–1284.
McCave, I.N., 1985. Properties of suspended sediment over the HEBBLE area on the Nova Scotia rise. Mar. Geol. 66, 169–188.
McCave, I.N., 2008. Size sorting during transport and deposition of fine sediments: Sortable silt and flow speed. In: Rebesco, M., Camerlenghi, A. (Eds.), Contourites. Elsevier, Amsterdam, pp. 121–142.
McCave, I.N., Manighetti, B., Beveridge, N.A.S., 1995. Circulation in the glacial North Atlantic inferred from grain-size measurements. Nature 374, 149–152.
Miguez-Salas, O., Rodríguez-Tovar, F.J., de Weger, W., 2020. *Macaronichnus* and contourite depositional settings: Bottom currents and nutrients as coupling factors. Palaeogeogr. Palaeoclimatol. Palaeoecol. 545 (8), 109639. https://doi.org/10.1016/j.palaeo.2020.109639.
Mulder, T., 2011. Sedimentary processes and their deposits. In: Huneke, H., Mulder, T. (Eds.), Deep-Sea Sediments, Developments in Sedimentology, vol. 63. Elsevier, Amsterdam, pp. 25–148.
Mulder, T., Syvitski, J.P.M., Migeon, S., Faugères, J.-C., Savoye, B., 2003. Marine hyperpycnal flows: Initiation, behavior and related deposits. A review. Mar. Pet. Geol. 20, 861–882.
Munier, T., Deconinck, J.-F., Pellenard, P., Hesselbo, S.P., Riding, J.B., Ullmann, C.V., Bougeault, C., Mercuzot, M., Santoni, A.-L., Landrein, P., Huret, E., 2021. Million-year-scale alternation of warm-humid and semi-arid periods as a mid-latitude climate mode in the early Jurassic (late Sinemurian, Laurasian Seaway). Clim. Past 17, 1547–1566.
Nara, M., 2006. Reappraisal of *Schaubcylindrichnus*: a probable dwelling/feeding structure of a solitary funnel feeder. Palaeogeogr. Palaeoclimatol. Palaeoecol. 240, 439–452.
Naruse, H., Nifuku, K., 2008. Three-dimensional morphology of the ichnofossils *Phycosiphon incertum* and its implication for paleoslope inclination. Palaios 23, 270–279.
Negi, J.G., Tiwari, R.K., 1984. Periodicities of palaeomagnetic intensity and palaeoclimatic variations: a Walsh spectral approach. Earth Planet. Sci. Lett. 70, 139–147.
Negi, J.G., Tiwari, R.K., Rao, K.N., 1993. Comparison of Walsh and Fourier spectroscopy of geomagnetic reversals and nonsinusoidal palaeoclimatic time series. IEEE Trans. Geosci. Remote Sens. 31, 127–135.
Kent, D.V., Olsen, P.E., Rasmussen, C., Lepre, C., Mundil, R., Irmis, R.B., Gehrels, G.E., Giesler, D., Geissman, J.W., Parker, W.G., 2018. Empirical evidence for stability of the 405-kiloyear 770 Jupiter-Venus eccentricity cycle over hundreds of millions of years. Proc. Natl. Acad. Sci. U. S. A. 115, 6153–6158.
Paczesna, J., 1996. The Vendian and Cambrian ichnocoenoses from the polish of the East-European Platform. Prace Państw. Inst. Geol. 153, 1–77.
Paillard, D., 2010. Climate and the orbital parameters of the Earth. Compt. Rendus Geosci. 342, 273–285.
Pemberton, G.S., Frey, R.W., 1982. Trace fossil nomenclature and the *Planolites–Palaeophycus* dilemma. J. Paleont. 56, 843–881.
Pemberton, G.S., Spila, M., Pulham, A.J., Saunders, T., MacEachern, J.A., Robbins, D., Sinclair, I.K., 2001. Ichnology & Sedimentology of shallow to marginal marine systems: Ben Nevis & Avalon Reservoirs, Jeanne D'Arc Basin. In: Geological Association of Canada, Short Course Notes, 15 (343 pp).
Pemberton, S.G., MacEachern, J.A., Dashtgard, S.E., Bann, K.L., Gingras, M.K., Zonneveld, J.-P., 2012. Shorefaces. In: Knaust, D., Bromley, R.G. (Eds.), Trace Fossils as Indicators of Sedimentary Environments, Developments in Sedimentology, vol. 64, pp. 563–604.
Pervesler, P., Uchman, A., 2004. Ichnofossils from the type area of the Grund Formation (Miocene, lower Badenian) in northern Lower Austria (Molasse Basin). Geol. Carpath. 55, 103–110.
Pervesler, P., Uchman, A., Hohenegger, J., 2008. New methods for ichnofabric analysis and correlation with orbital cycles exemplified by the Baden-Sooss section (Middle Miocene, Vienna Basin, Lower Austria). Geol. Carpath. 59, 395–409.
Pieńkowski, G., 1985. Early Liassic trace fossils assemblages from the Holy Cross Mountains, Poland: Their distribution in continental and marginal marine environments. In: Curran, A.H. (Ed.), Biogenic Structures: Their Use in Interpreting Depositional Environments, Soc. Econ. Paleont. Miner. Spec. Publ, vol. 35, pp. 37–51.
Pieńkowski, G., 2004. The epicontinental lower Jurassic of Poland. Pol. Geol. Inst. Sp. Pap. 12, 1–154.
Pollard, J.E., 1988. Trace fossils in coal-bearing sequence. J. Geol. Soc. Lond. 145, 339–350.
Powell, J.H., 2010. Jurassic sedimentation in the Cleveland Basin: a review. Proc. Yorks. Geol. Soc. 58, 21–72.
Raine, R., Copestake, P., Simms, M.J., Boomer, I., 2020. Uppermost Triassic to lower Jurassic sediments of the island of Ireland and its surrounding basins. Proc. Geol. Assoc. https://doi.org/10.1016/j.pgeola.2020.04.001.
Rebesco, M., Wåhlin, A., Laberg, J.S., Schauer, A., Brezcynska-Möller, A., Lucchi, R.G., Noormets, R., Accettella, D., Zarayskaya, Y., Diviacco, P., 2013. Quaternary contourite drifts of the Western Spitsbergen margin. Deep-Sea Res. Part I: Oceanogr. Res. Pap. 79, 156–168.
Rebesco, M., Hernández-Molina, F.J., Van Rooij, D., Wåhlin, A., 2014. Contourites and associated sediments controlled by deep-water circulation processes: state of the art and future considerations. Mar. Geol. 352, 111–154.
Rodríguez-Tovar, F.J., 2014. Orbital climate cycles in the fossil record: from semidiurnal to million-year biotic responses. Annu. Rev. Earth Planet. Sci. 42, 69–102.
Rodríguez-Tovar, F.J., Hernández-Molina, F.J., 2018. Ichnological analysis of contourites: Past, present and future. Earth-Sci. Rev. 182, 28–41.
Rodríguez-Tovar, F.J., Löwemark, L., Pardo-Igúzquiza, E., 2011. *Zoophycos* cyclicity during the last 425 ka in the northeastern South China Sea: evidence for monsoon fluctuation at the Milankovitch scale. Palaeogeogr. Palaeoclimatol. Palaeoecol. 305, 256–263.
Rodríguez-Tovar, F.J., Nagy, J., Reolid, M., 2014. Palaeoenvironment of Eocene prodelta in Spitsbergen recorded by the trace fossil *Phycosiphon incertum*. Polar Res. 33, 23786. https://doi.org/10.3402/polar.v33.23786.
Rodríguez-Tovar, F.J., Mena, A., Hernández-Molina, F.J., Dorador, J., 2016. Incidence of bioturbation on grain size redistribution: preventing misinterpretations in sedimentary analysis. GeoTemas 16, 291–294.
Rodríguez-Tovar, F.J., Dorador, J., Mena, A., Hernández-Molina, F.J., 2017. Improving Ichnofabric Analysis in Cores: Computed Tomography Images and High Resolution Digital Treatment. In: 14th International Ichnofabric Workshop, Taipei, Taiwan. TPE, Taipei, p. 47.
Rodríguez-Tovar, F.J., Hernández-Molina, F.J., Hüneke, H., Llave, E., Stowe, D., 2019. Contourite facies model: improving contourite characterization based on the ichnological analysis. Sediment. Geol. 384, 60–69.
Rodríguez-Tovar, F.J., Pardo-Igúzquiza, E., Reolid, M., 2020. Cyclic environmental changes during the early Toarcian at the Mochras Farm Borehole (Wales): a variable response of the foraminiferal community. Lethaia 54, 113–126. https://doi.org/10.1111/let.12392.
Ruebsam, W., Reolid, M., Sabatino, N., Masetti, D., Schwark, L., 2020. Molecular paleothermometry of the early Toarcian climate perturbation. Glob. Planet. Chang. 195, 103351. https://doi.org/10.1016/j.gloplacha.2020.103351.
Ruhl, M., Hesselbo, S.P., Hinnov, L., Jenkyns, H.C., Xu, W., Storm, M.S., Riding, J.B., Minisini, D., Ullmann, C.V., Leng, M.J., 2016. Astronomical constraints on the duration of the early Jurassic Pliensbachian Stage and global climatic fluctuations. Earth Planet. Sci. Lett. 455, 149–165.
Ruvalcaba Baroni, I., Pohl, A., van Helmond, N.A.G.M., Papadomanolaki, N.M., Coe, A. L., Cohen, A.S., van de Schootbrugge, B., Donnadieu, Y., Slomp, C.P., 2018. Ocean Circulation in the Toarcian (early Jurassic): a Key Control on Deoxygenation and Carbon Burial on the European Shelf. Paleoceanogr. Paleoclimat. 33, 994–1012.
Salter, J.W., 1857. On annelide-burrows and surface-markings from the Cambrian rocks of the Longmynd. Q. J. Geol. Soc. Lond. 13, 199–206.
Savarese, M., Dodd, J.R., Lane, N.G., 1997. Taphonomic and sedimentologic implications of crinoid intraskeletal porosity. Lethaia 29, 141–156.
Savrda, C.E., 1995. Ichnologic applications in paleoceanographic, paleoclimatic, and sea-level studies. Palaios 10, 565–577.
Savrda, C.E., Bottjer, D.J., 1994. Ichnofossils and ichnofabrics in rhythmically bedded pelagic/hemi-pelagic carbonates: recognition and evaluation of benthic redox and scour cycles. Spec. Publ. Int. Ass. Sediment. 19, 195–210.
Savrda, C.E., Krawinkel, H., McCarthy, F.M.G., McHugh, C.M.G., Olson, H.C., Mountain, G., 2001. Ichnofabrics of a Pleistocene slope succession, New Jersey in relation to climate and sea-level dynamics. Palaeogeogr. Palaeoclimatol. Palaeoecol. 171, 41–61.
Schlirf, M., 2000. Upper Jurassic trace fossils from the Boulonnais (northern France). Geol. Palaeontol. 34, 145–213.
Schlirf, M., Uchman, A., 2005. Revision of the ichnogenus *Sabellarifex* Richter, 1921 and its relationship to *Skolithos* Haldeman, 1840 and *Polykladichnus* Fürsich, 1981. J. Syst. Palaeont. 3, 115–131.
Seilacher, A., 1955. Spuren und Fazies im Unterkambrium. In: Schindewolf, O.H., Seilacher, A. (Eds.), Beiträge zur Kenntnis des Kambriums in der Salt Range (Pakistan). Akad. Wissensch. Literat. Mainz. Abh. Math.-naturwissenschaft. Kl, 10, pp. 373–399.
Seilacher, A., 2007. Trace Fossil Analysis. Springer, Berlin (226 pp).
Sellwood, B.W., 1972. Regional environmental changes across a lower Jurassic stage-boundary in Britain. Palaeontology 15, 125–157.
Shanmugam, G., 2000. 50 years of the turbidite paradigm (1950s–1990s), deep-water processes and facies models – a critical perspective. Mar. Pet. Geol. 17, 285–342.
Shanmugam, G., 2008. Deep-water bottom currents and their deposits. In: Rebesco, M., Camerlenghi, A. (Eds.), Contourites: Developments in Sedimentology, 60. Elsevier, Amsterdam, pp. 59–83.
Shanmugam, G., 2017. Contourites: Physical oceanography, process sedimentology, and petroleum geology. Pet. Explor. Dev. 44, 183–216.
Stachacz, M., 2016. Ichnology of the Cambrian Ociesęki Sandstone Formation (Holy Cross Mountains, Poland). Ann. Soc. Geol. Pol. 86, 291–328.

Stanistreet, I.G., Le Blanc Smith, G.K., Cadle, A.B., 1980. Trace fossils as sedimentological and palaeoenvironmental indices in the Ecca Group (lower Permian) of the Transvaal. Trans. Geol. Soc. S. Afr. 83, 333–344.
Storm, M.S., Hesselbo, S.P., Jenkyns, H.C., Ruhl, M., Ullmann, C.V., Xu, W., Leng, M.J., Riding, J.B., Gorbanenko, O., 2020. Orbital pacing and secular evolution of the early Jurassic carbon cycle. Proc. Natl. Acad. Sci. U. S. A. 117, 3974–3982. https://doi.org/10.1073/pnas.1912094117.
Stow, D.A.V., Faugères, J.C., 2008. Contourite facies and the facies model. In: Rebesco, M., Camerlenghi, A. (Eds.), Contourites, Developments in Sedimentology, vol. 60. Elsevier, Amsterdam, pp. 223–256.
Stow, D.A.V., Holbrook, J.A., 1984. North Atlantic contourites: An overview. In: Stow, D.A.V., Piper, D.J.W. (Eds.), Fine-Grained Sediments, Deep-Water Processes and Facies, Geol. Soc. London Spec. Publ, vol. 15, pp. 245–256.
Stow, D.A.V., Faugères, J.-C., Howe, J.A., Pudsey, C.J., Viana, A.R., 2002. Bottom currents, contourites and deep-sea sediment drifts: Current state-of-the-art. In: Stow, D.A.V., Pudsey, C.J., Howe, J.A., Faugères, J.-C., Viana, A.R. (Eds.), Deep-Water Contourite Systems: Modern Drifts and Ancient Series, Seismic and Sedimentary Characteristics, vol. 22, pp. 7–20. Geol. Soc., London, Mem.
Suess, E., 1980. Particulate organic carbon flux in the oceans – surface productivity and oxygen utilization. Nature 288, 260–263.
Surlyk, F., Lykke-Andersen, H., 2007. Contourite drifts, moats and channels in the late cretaceous chalk of the Danish Basin. Sedimentology 54, 405–422.
Taylor, A., Goldring, R., Gowland, S., 2003. Analysis and application of ichnofabrics. Earth-Sci. Rev. 60, 227–259.
Thistle, D., Yingst, J.Y., Fauchald, K., 1985. A deep-sea benthic community exposed to strong near-bottom currents on the Scotian rise (western Atlantic). Mar. Geol. 66, 91–112.
Thistle, D., Ertman, S.C., Fauchald, K., 1991. The fauna of the HEBBLE site: patterns in standing stock and sediment-dynamic effects. Mar. Geol. 99, 413–422.
Tiwari, R.K., 1987. A Walsh spectral comparison of oxygen (δ18O) and carbon isotope (δ13C) variations of the Pleistocene bore hole (Eureka 67–135) from the Gulf of Mexico and their orbital significance. Mar. Geol. 78, 167–174.
Torell, O.M., 1870. Petrifacta Suecana formationis Cambricae. Lunds Univ. Årsskrift 6 (pt. 2), 1–14 n. 8.
Tucholke, B.E., Hollister, C.D., Biscaye, P.E., Gardner, W.D., 1985. Abyssal current character determined from sediment bedforms on the Nova Scotian continental rise. Mar. Geol. 66, 43–57.
Uchman, A., 1992. Ichnogenus *Rhizocorallium* in the Paleogene flysch (Outer Western Carpathians, Poland). Geol. Carpath. 43, 57–60.
Uchman, A., 1995. Taxonomy and palaeoecology of flysch trace fossils: the Marnoso-arenacea Formation and associated facies (Miocene, Northern Apennines, Italy). Beringeria 15, 3–115.
Uchman, A., 1998. Taxonomy and ethology of flysch trace fossils: a revision of the Marian Książkiewicz collection and studies of complementary material. Ann. Soc. Geol. Pol. 68, 105–218.
Uchman, A., 1999. Ichnology of the Rhenodanubian Flysch (lower Cretaceous–Eocene) in Austria and Germany. Beringeria 25, 65–171.
Uchman, A., Tchoumatchenco, P., 2003. A mixed assemblage of deep-sea and shelf trace fossils from the lower cretaceous (Valanginian) Kamchia Formation in the Troyan region, central Fore-Balkan, Bulgaria. Ann. Soc. Geol. Pol. 73, 27–34.
Uchman, A., Wetzel, A., 2011. Deep-sea ichnology: The relationships between depositional environment and endobenthic organisms. In: Hüneke, H., Mulder, T. (Eds.), Deep-Sea Sediments, Developments in Sedimentology, vol. 63, pp. 517–556.
Ullmann, C.V., Szűcs, D., Jiang, M., Hudson, A.J.L., Hesselbo, S.P., 2021. Geochemistry of macrofossil, bulk rock, and secondary calcite in the Early Jurassic strata of the Llanbedr (Mochras Farm) drill core, Cardigan Bay Basin, Wales, UK. J. Geol. Soc. Lond. https://doi.org/10.1144/jgs2021-018 (Published early online).
Valdes, P.J., Glover, R.W., 1999. Modelling the climate response to orbital forcing. Phil. Trans. Royal Soc. London. Ser. A 357 (1757), 1873–1890.
Van Buchem, F.S.P., Knox, R.W.O., 1998. Lower and Middle Liassic depositional sequences of Yorkshire (U.K.). In: de Graciansky, P.C., Hardenbol, J., Jacquin, T., Vail, P.R. (Eds.), Mesozoic and Cenozoic Sequence Stratigraphy of European Basins. SEPM Spec. Publ, 60. Soc. Sediment. Geol, Tulsa, Okla, pp. 545–559.
Van Buchem, F.S.P., McCave, I.N., 1989. Cyclic sedimentation patterns in lower Lias mudstones of Yorkshire (GB). Terra Nova 1, 461–467.
Van Buchem, F.S.P., McCave, I.N., Weedon, G.P., 1994. Orbitally induced small scale cyclicity in a siliciclastic epicontinental setting (Cleveland Basin, lower Lias, Yorkshire, UK). In: de Boer, P.L., Smith, D.G. (Eds.), Orbital Forcing and Cyclic Sedimentary Sequences, Spec. Publ. Internat. Assoc. Sedimentol, vol. 19, pp. 345–366.
Van de Schootbrugge, B., Bailey, T.R., Rosenthal, Y., Katz, M.E., Wright, J.D., Miller, K. G., Feist-Burkhardt, S., Falkowski, P.G., 2005. Early Jurassic climate change and the radiation of organic-walled phytoplankton in the Tethys Ocean. Paleobiology 31, 73–97.
Van de Schootbrugge, B., Houben, A.J.P., Ercan, F.E.Z., Verreussel, R., Kerstholt, S., Janssen, N.M.M., Nikitenko, B., Suan, G., 2019. Enhanced Arctic-Tethys connectivity ended the Toarcian Oceanic Anoxic Event in NW Europe. Geol. Mag. 157, 1593–1611. https://doi.org/10.1017/S0016756819001262.
Van Echelpoel, E., 1994. Identification of regular sedimentary cycles using Walsh spectral analysis with results from the Boom Clay Formation, Belgium. In: de Boer, P. L., Smith, D. (Eds.), Orbital Forcing and Cyclic Sequences, Spec. Publ. Internat. Assoc. Sedimentol, vol. 19, pp. 63–76.
Van Rooij, D., Iglesia, J., Hernández-Molina, F.J., Ercilla, G., Gomez-Ballesteros, M., Casas, D., Llave, E., De Hauwere, A., Garcia-Gil, S., Acosta, J., Henriet, J.-P., 2010. The Le Danois contourite depositional system: Interactions between the Mediterranean Outflow Water and the upper Cantabrian slope (North Iberian margin). Mar. Geol. 274, 1–20.
Vandorpe, T., Van Rooij, D., Stow, D.A.V., Henriet, J.-P., 2011. Pliocene to recent shallow-water contourite deposits on the shelf and shelf edge off south-western Mallorca, Spain. Geo-Marine Lett. 31, 391–403.
Voigt, E., Häntzschel, W., 1956. Die grauen Bänder in der Schreibkreide Nordwest-Deutschlands und ihre Deutung als Lebensspuren. Mitt. Geol. Staatsinst. Hamburg 25, 104–122.
Wang, Y., Wang, X., Hu, B., Uchman, A., 2019. Burrows of the polychaete *Perinereis aibuhiutensis* on a tidal flat of Yellow River Delta in China: Implications for the ichnofossils *Polykladichnus* and *Archaeonassa*. Palaios 34, 271–279.
Weedon, G., 1989. The detection and illustration of regular sedimentary cycles using Walsh power spectra and filtering, with examples from the Lias of Switzerland. J. Geol. Soc. 146, 133–144.
Weedon, G., 2003. Time-Series Analysis and Cyclostratigraphy: Examining Stratigraphic Records of Environmental Cycles. Cambridge University Press, Cambridge (259 pp).
Weedon, G., Read, W.A., 1995. Orbital-climatic forcing of Namurian cyclic sedimentation from spectral analysis of the Limestone Coal Formation, Central Scotland. Geol. Soc. London Spec. Publ. 85, 51–66.
Westergård, A.H., 1931. Diplocraterion, *Monocraterion* and *Scolithus*. Sver. Geol. Undersöknig Årsbok Ser. C 25, 3–25.
Wetzel, A., 1981. Ökologische und stratigraphische Bedeutung biogener Gefüge in quartären Sedimenten am NW-afrikanischen Kontinentalrand. In: "Meteor" Forsch.-Ergebnisse, Reihe C, 34, pp. 1–47.
Wetzel, A., 1983. Biogenic structures in modern slope to deep-sea sediments in the Sulu Sea Basin (Philippines). Palaeogeogr. Palaeoclimatol. Palaeoecol. 42, 285–304.
Wetzel, A., 1991. Ecologic interpretation of deep-sea trace fossil communities. Palaeogeogr. Palaeoclimatol. Palaeoecol. 85, 47–69.
Wetzel, A., 2007. Ichnofabrics in Eocene to Maestrichtian sediments from Deep Sea Drilling Project Site 605, off the New Jersey coast. Deep Sea Drill. Proj. Rep. Publ. 93, 825–835.
Wetzel, A., 2010. Deep-sea ichnology: Observations in modern sediments to interpret fossil counterparts. Acta Geol. Pol. 60, 125–138.
Wetzel, A., Bromley, R.G., 1994. *Phycosiphon incertum* revisited: *Anconichnus horizontalis* is its junior subjective synonym. J. Paleont. 68, 1396–1402.
Wetzel, A., Uchman, A., 2001. Sequential colonization of muddy turbidites: examples from Eocene Beloveža Formation, Carpathians, Poland. Palaeogeogr. Palaeoclimatol. Palaeoecol. 168, 171–186.
Wetzel, A., Uchman, A., 2012. Hemipelagic and pelagic basin plains. In: Bromley, R.G., Knaust, D. (Eds.), Trace Fossils as Indicators of Sedimentary Environments, Developments in Sedimentology, vol. 64. Elsevier, Amsterdam, pp. 673–701.
Wetzel, A., Werner, F., 1981. Morphology and ecological significance of *Zoophycos* in deep-sea sediments off NW Africa. Palaeogeogr. Palaeoclimatol. Palaeoecol. 32, 185–212.
Wetzel, A., Blechschmidt, I., Uchman, A., Matter, A., 2007. A highly diverse ichnofauna in late Triassic deep-sea fan deposits of Oman. Palaios 22, 567–576.
Wetzel, A., Werner, F., Stow, D.A.V., 2008. Bioturbation and biogenic sedimentary structures in contourites. In: Rebesco, M., Camerlenghi, A. (Eds.), Contourites, Developments in Sedimentology, vol. 60. Elsevier, Amsterdam, pp. 183–202.
Wignall, P.B., 1991. Dysaerobic trace fossils and ichnofabrics in the Upper Jurassic Kimmeridge Clay of Southern England. Palaios 6, 264–270.
Woodland, A.W. (Ed.), 1971. The Llanbedr (Mochras Farm) Borehole. Report No. 71/18, Institute of Geological Sciences (115 pp).
Xu, W., Ruhl, M., Jenkyns, H.C., Leng, M.J., Huggett, J.M., Minisini, D., Ullmann, C.V., Riding, J.B., Weijers, J.W.H., Storm, M.S., Percival, L.M.E., Tosca, N.J., Idiz, E.F., Tegelaar, E.W., Hesselbo, S.P., 2018. Evolution of the Toarcian (early Jurassic) carbon-cycle and global climatic controls on local sedimentary processes (Cardigan Bay Basin, UK). Earth Planet. Sci. Lett. 484, 396–411.
Zhang, L.-J., Fan, R.-Y., Gong, Y.-M., 2015. *Zoophycos* macroevolution since 541 Ma. Nat. Sci. Rep. 5 (14954), 1–10. https://doi.org/10.1038/srep14954, www.nature.com/scientificreports/.